

POLITECNICO DI TORINO

MASTER'S DEGREE IN MECHATRONIC
ENGINEERING

DEPARTMENT OF CONTROL AND COMPUTER ENGINEERING

MASTER'S DEGREE THESIS

**Dynamic modeling of induction motors in
developing tool for automotive
applications**



Academic Supervisors:

Prof. Alberto TENCONI
Prof. Silvio VASCHETTO
Ing. Ornella STISCIA

Company Supervisor:

Dott. Giulio BOCCARDO

Candidate:

Roberta LE FOSSE

A.Y. 2020/2021

*"Our greatest weakness lies in giving up. The most certain
way to succeed is always to try just one more time"*
Thomas Edison

Abstract

The current electrification processes involving hybrid and electric vehicles require increasingly accurate tools to evaluate electric powertrain performance and reliability. In this context, the virtualization of electric powertrain components needs to be performed. In this way, several analyses like energetic assessments can be performed without using physical components, saving costs and development times.

Among the virtualization methods, an ever more used simulation approach in automotive industries consists of the Hardware in the Loop (HIL). The HIL is a real-time simulation method that allows testing one or more real components of an electric powertrain without the need for the other hardware components usually connected to it. For example, using HIL makes it possible to test a motor control unit without connecting to it a real electronic power converter or even an electrical machine. Hence, the main advantages of this simulation approach are evident.

In this thesis, the HIL simulation approach is used to virtualize the electric machine of a hybrid or electric powertrain. The simulation hardware consists of the dSPACE rapid prototyping board and using the library “XSG Electric Library” provided by dSPACE. The work activity has been developed through the cooperation between Politecnico di Torino and POWERTECH ENGINEERING S.r.l., a consulting company specialized in simulation and development of conventional powertrains, and more recently, hybrid and electric ones, too.

This thesis focuses on the validation and analysis of dynamic models for electrical machines using dSPACE. The considered components are the Induction Machine (IM) and, like side-activity, the Voltage Source Inverter (VSI). Concerning the IM, it has been modeled using the following reference frames: phase values time-domain (abc), stationary axes ($\alpha\beta 0$), and rotating rotor flux (dq) axes. The aim of the work was the comparison of the models, so the iron losses and the magnetic saturation were neglected. Also, to handle and figure out the models, their analysis and validation have been performed in the Matlab/Simulink environment. Thus, comparing the obtained responses with those provided by dSPACE. Finally, the VSI has been modelled considering its average behaviour, without considering the Pulse Width Modulation (PWM), and so making the models’ simulations faster to be performed.

A real IM has been tested on a dedicated test rig in Politecnico di Torino’s laboratories to get a preliminary validation of the proposed models. The IM parameters have been obtained by performing the standard no-load and locked rotor tests.

Contents

Abstract

List of Figures **iii**

List of Tables **v**

1	Introduction	1
1.1	Hardware in the Loop	3
1.2	Thesis goal	4
2	Induction motor modeling	5
2.1	Squirrel cage induction motor	5
2.2	Mathematical model in phase variable domain	6
2.3	Mathematical model in stationary reference frame ($\alpha\beta$)	10
2.4	Mathematical model in rotating reference frame (dq)	13
2.5	Equivalent circuit in rotating coordinates	16
2.6	Induction machine model	20
2.7	Test of induction machine	21
	2.7.1 No-load test	21
	2.7.2 Locked-rotor test	23
2.8	Mathematical model of Voltage Source Inverter (VSI)	24
3	Simulink and dSPACE comparisons in stationary reference frame ($\alpha\beta$)	29
3.1	Overview on Simulink model	30
3.2	dSPACE general description	32
3.3	Overview on dSPACE model	35
3.4	Simulink and dSPACE results comparison	41
	3.4.1 Simulation: 220V - 50Hz	42
	3.4.2 Simulation: 380V - 40Hz	47
4	Real-time simulations	52
4.1	FPGA build process	53

4.2	Comparison between Simulink and dSPACE real-time simulations ($\alpha\beta$) reference frame	54
4.3	Comparison between Simulink and dSPACE real-time simulations (dq) reference frame	57
5	Validation of the dynamic model	65
5.1	Model of the system	65
5.2	Calculation of machine parameters	67
5.3	Validation of experimental data	70
6	Conclusions and next steps	75
	Bibliography	78

List of Figures

1.1	POWERTECH Engineering.	2
1.2	Workstation.	2
1.3	SCALEXIO LabBox and Oscilloscope.	3
2.1	Structure of Induction machine (Rik De Doncker, 2011) [3].	6
2.2	Winding distribution of three-phase Induction Motor.	8
2.3	Machine model in stationary reference frame ($\alpha\beta$).	10
2.4	Equivalent circuit in the (dq) rotor reference frame.	17
2.5	Rotor flux vector in (dq) coordinates.	18
2.6	Stator and Rotor current vectors in (dq) coordinates (steady-state conditions).	19
2.7	Equivalent circuit in (dq) reference frame.	20
2.8	Equivalent circuit of the no-load test.	22
2.9	Equivalent circuit of the no-load test.	23
2.10	Three-phase inverter.	24
2.11	Voltage vectors.	26
2.12	Voltage Source Inverter.	27
2.13	Modulation indices.	28
2.14	Voltage.	28
3.1	Scheme of the model.	30
3.2	Simulink ($\alpha\beta$) model.	31
3.3	Induction Motor Simulink ($\alpha\beta$) model.	31
3.4	Mechanic Simulink model.	32
3.5	Single-Model Approach [7].	33
3.6	Double-Model Approach [7].	33
3.7	DS6602 FPGA Base Board [8].	34
3.8	SCALEXIO LabBox [7].	35
3.9	dSPACE processor interface.	36
3.10	dSPACE FPGA interface.	36
3.11	Buffer2Register and Register2Buffer blocks [9].	37
3.12	Processor part and FPGA part direct communication [9].	38
3.13	SCIM Machine block FPGA interface.	39
3.14	Mechanic block FPGA interface.	40
3.15	Stator Currents i_a - 220V-50Hz.	44
3.16	Electrical and Mechanical Powers - 220V-50Hz.	44
3.17	Motor Torque - 220V-50Hz - 220V-50Hz.	45
3.18	Rotor Speed - 220V-50Hz.	45
3.19	Rotor Flux - 220V-50Hz.	46

3.20	Stator Flux - 220V-50Hz.	46
3.21	Stator Currents i_a - 380V-40Hz.	48
3.22	Electrical and Mechanical Powers - 380V-40Hz.	49
3.23	Motor Torque - 380V-40Hz.	49
3.24	Rotor Speed - 380V-40Hz.	50
3.25	Rotor Flux - 380V-40Hz.	50
3.26	Stator Flux - 380V-40Hz.	51
4.1	FPGA Setup and System Generator.	53
4.2	ConfigurationDesk interface.	53
4.3	ControlDesk interface.	54
4.4	FPGA model comment out.	55
4.5	Stator current Simulink and dSPACE real-time.	56
4.6	Rotor speed Simulink and dSPACE real-time.	56
4.7	Simulink (dq) model.	57
4.8	Induction Motor Simulink (dq) model.	58
4.9	Calculate of Mechanical Power dSPACE (dq) model.	60
4.10	Zoom on the blocks to calculate of Mechanical Power dSPACE (dq) model.	61
4.11	Mechanical Power dSPACE (dq) model block.	61
4.12	Stator current Simulink and dSPACE real-time (dq) model.	62
4.13	Stator current d-axis Simulink and dSPACE real-time (dq) model.	63
4.14	Stator current q-axis Simulink and dSPACE real-time (dq) model.	63
4.15	Rotor Speed Simulink and dSPACE real-time (dq) model.	64
5.1	HBM and Single-three phase power source 40kVA.	66
5.2	Induction motor and Current transducers.	66
5.3	Schematic representation of the test bench.	67
5.4	Instrumentations used during the no-load and locked rotor tests.	68
5.5	Stator Current 30V - 50Hz with ramp acceleration.	71
5.6	Zoom starting transient - Stator current 30V - 50Hz with ramp acceleration.	72
5.7	Zoom steady state - Stator current 30V - 50Hz with ramp acceleration.	72
5.8	Stator Current 30V - 50Hz with step acceleration	73
5.9	Zoom starting transient - Stator current 30V - 50Hz with step acceleration.	73
5.10	Zoom steady state - Stator current 30V - 50Hz with step acceleration.	74

List of Tables

3.1	Characteristics of the motor.	41
3.2	Parameters of the Induction Motor.	41
3.3	Parameters of the Mechanic block.	42
3.4	Steady-state Simulink simulation - 220V-50Hz.	43
3.5	Steady-state dSPACE simulation - 220V-50Hz.	43
3.6	Steady-state Simulink simulation - 380V-40Hz.	47
3.7	Steady-state dSPACE simulation - 380V-40Hz.	48
5.1	Data of the IM.	68
5.2	No-load test results.	69
5.3	Locked-rotor test results.	69
5.4	Parameters of the Induction Motor FIMET HMA160L4.	70
5.5	Validation of experimental data.	70

Chapter 1

Introduction

Electrification of transport has become an important argument in recent years. Due to the emission of CO_2 , electric and hybrid vehicles are the most common challenges of the current period. For this reason, electrical machines will play an important role to produce zero-emissions vehicles [1].

In the industrial sector the three-phase Induction Motor (IM) is the most used machine, in fact, it accounts for 85% of all motors [2]. IM is characterized by low cost, weight and it is a very robust motor with respect to the DC motor.

To simulate electric motors are not used micro-controllers like CPU, but there is a need to use advanced technologies like FPGA.

Field Programmable Gate Arrays (FPGA) is a reprogrammable silicon chips and it can be configured in a specific way and thanks to this the execution time is reduced.

It has interconnections between logic gates that are combined to form a combinatorial logic block.

FPGA works with a very small time-step and in this work, the FPGA used works with a time-step of $8 \cdot 10^{-9}$ seconds.

FPGA can be used to simulate in real time (1 simulated second = 1 real second) complex systems with very low timescale such as the electromagnetic phenomena that occur in electronic and electric power motors. This allows to implement the Hardware in the Loop (HIL) simulation.

Instead, standard Simulink models of electrical machines, which run on standard CPU, are not in real-time (1 simulated second > 1 real second) and can not be used for HIL.

Real-time simulations were carried out in POWERTECH Engineering (PWT), an independent consulting company in the field of CFD-3D, 1D and XIL simulation. POWERTECH Engineering is a leading company in powertrain simulation engineering services. For several years, PWT has been investing in HIL simulations for validation, testing and virtual calibration of the ECU. To do this, it has equipped the dSPACE toolchain, strongly used for this type of simulations.



Figure 1.1: POWERTECH Engineering.

Thanks to the innovative workstation in PWT, it was possible to implement and validate the Squirrel cage Induction motor model.

The workstation is as follows:

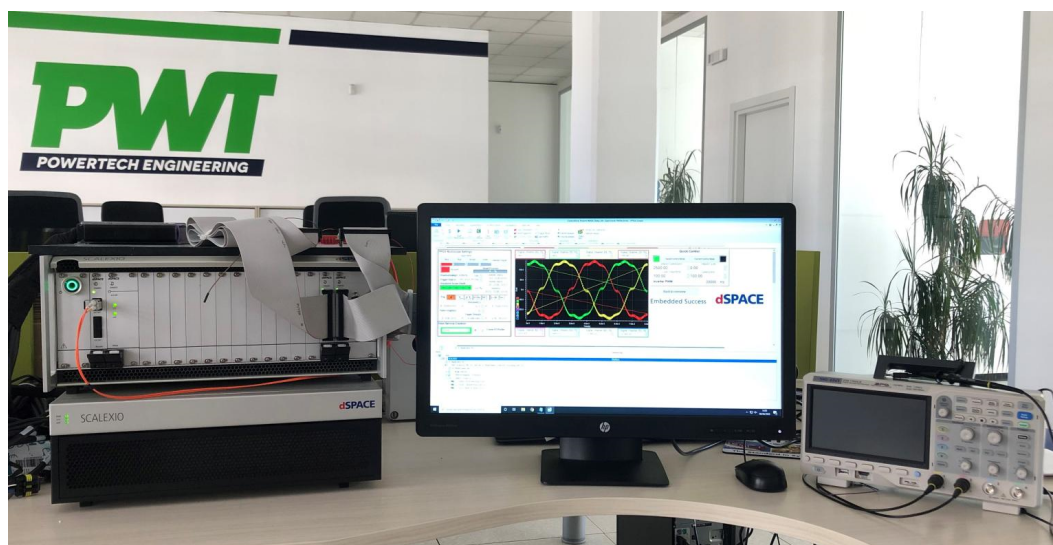


Figure 1.2: Workstation.

As is possible to see, on the left is the SCALEXIO LabBox and on the right the oscilloscope.

In the figure below, a zoom of the SCALEXIO LabBox and the oscilloscope:



Figure 1.3: SCALEXIO LabBox and Oscilloscope.

1.1 Hardware in the Loop

Hardware in the Loop (HIL) applications are tools used for simulations. These tools have improved in recent years thanks to the development of mechatronics and embedded systems. HIL includes all tests techniques of the mechanical and electrical control units. These units, in general, are connected to test benches. These test benches, very often, are difficult to realize because they are made up of different components, such as sensors and actuators.

The HIL simulations are widely used because they allow reproducing of these test benches, in order to anticipate the tests on the components, without being available the finished product. In fact, the components respond to the simulated signals as if operating in a real environment. This is possible because the HIL simulator failed to distinguish the real signals from those coming from a real-time simulation.

This allows observing the behaviour of individual components of the system that would be very difficult to observe in reality.

One of the advantages of HIL simulations is that it is possible to gradually analyse the components of a real system and to integrate different subsystems.

Due to the short simulation times, the lower costs and the safety of testing and the high accuracy of the model with respect to the reality, the use of these simulations has many advantages.

1.2 Thesis goal

The activity of this thesis work is the study and the implementation of the dynamic model of a squirrel cage induction machine. This model was first developed in Matlab/Simulink in $(\alpha\beta)$ and (dq) reference frames and then in dSPACE.

As side-activity also the Voltage Source Inverter (VSI) in Matlab/Simulink was developed. This model can be used to next activity, like the motor control.

The Matlab/Simulink and the dSPACE models were compared in off-line simulations and when they were perfectly overlapped the real-time simulations were performed. Also in this case, the models are compared.

As the last activity, the validation of experimental data was carried out.

Chapter 2

Induction motor modeling

This chapter describes the model of the Induction Motor (IM), called also “asynchronous machine”. The IM is the most used electric machine. It works directly connected to the electric network, for this reason, it is low expensive, very reliable and robust.

The mathematical model of the IM will be explained. In particular, to simplify the model the two-phase model will be obtained. We will see two reference frames:

- the fixed stator reference frame ($\alpha\beta$);
- the rotating synchronous reference frame with the rotor flux (dq).

2.1 Squirrel cage induction motor

In the Figure is shown the structure of the squirrel cage induction motor (SCIM). The SCIM is made by a conductors these are colour in red. These are short-circuited by a conductive ring at both ends and has 4 poles. The stator circuit generates a magnetic field that penetrates the rotor circuit. The purpose of this magnetic field is to create an asynchronous speed respect at the stator speed at the alternating currents performed. These currents and stator field will generate the torque of the motor.

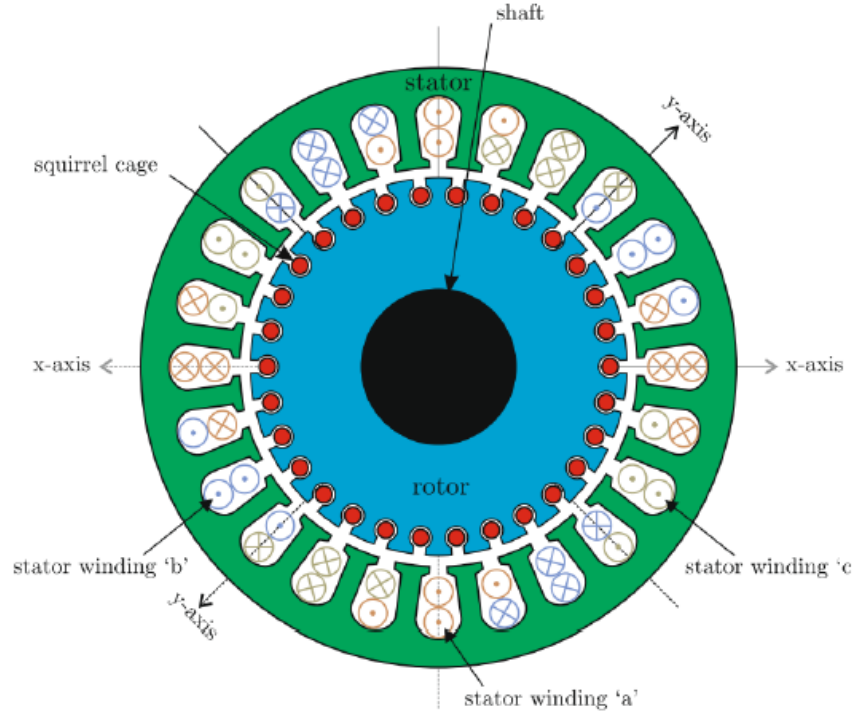


Figure 2.1: Structure of Induction machine (Rik De Doncker, 2011) [3].

2.2 Mathematical model in phase variable domain

The IM works below the synchronous speed in the motor operation and above in the generator operation.

The magnetomotive force (mmf) is generated by a balanced set of three-phase currents that flowing in a symmetrical set of three-phase windings [4]:

$$F(\theta_a^e, t) = \frac{3}{2} \cdot \frac{4}{\pi} \cdot \frac{N}{2P} \cdot I_m \cdot \cos(\theta_a^e - \omega_e t) \quad (2.1)$$

where:

- θ_a^e is the electrical angle (deg);
- ω_e is the angular speed of the stator mmf (rad/s). It depends on the frequency f and I_m that is the excitation currents;
- P is the number of the pole pairs.

In the next equation, we can see the synchronous speed (rad/s):

$$\omega_s = \frac{\omega_e}{P} \quad (2.2)$$

To evaluate the revolution per minute (rpm):

$$n_s = \frac{60 \cdot f}{P} \quad (2.3)$$

When the rotor is rotating there is also the rotor speed (rad/s). Between synchronous speed and rotor speed, there is a slip. It is defined in the following way:

$$\omega_{slip} = \omega_s - \omega_r \quad (2.4)$$

The slip speed can be expressed:

$$s = \frac{\omega_s - \omega_r}{\omega_s} = \frac{\omega_e - \omega_r}{\omega_e} \quad (2.5)$$

The slip speed can also be expressed as $\omega_{slip} = s \cdot \omega_s$ and s can be positive and negative in the generator operation because the rotor speed is higher than the synchronous speed.

When the rotor circuit is closed, the mmf generated the rotor voltages and these generate currents. The magnitude of the currents depends on the induced rotor voltages and by the rotor circuit impedance.

When the ω_r is zero, the motor accelerates with the synchronous speed and the slip frequency decreases. Like the stator currents, also the rotor currents establish their mmf revolving field with a speed equal to $s \cdot \omega_s$. The rotor has a speed equal to ω_r , so the absolute speed of the rotor mmf field is:

$$\omega_r + s \cdot \omega_s = \omega_s \quad (2.6)$$

A constant torque will be produced in steady-state conditions, for the reason that the stator

and the rotor *mmf* rotate at the same speed.

Now, we consider the magnetic stator and rotor circuit, as shown in Figure 2.2:

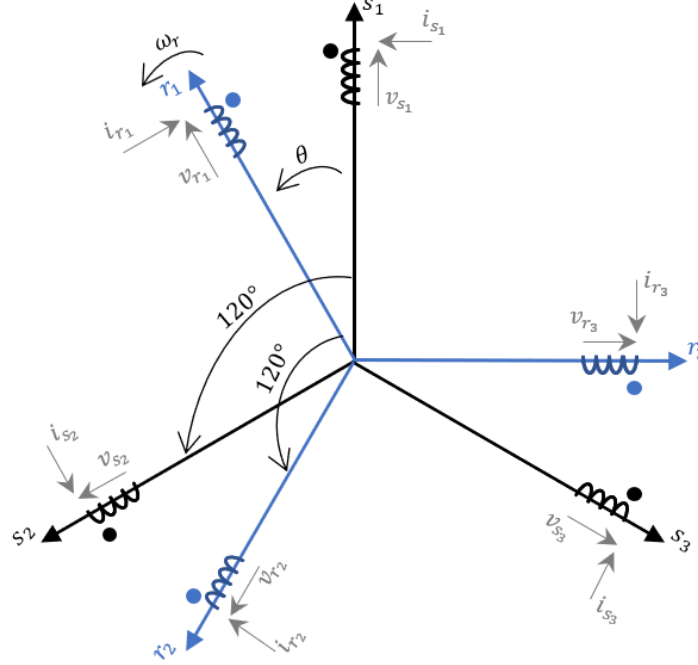


Figure 2.2: Winding distribution of three-phase Induction Motor.

The stator voltage equations are the following:

$$\bar{v}_{s123} = R_s \cdot \bar{i}_{s123} + \frac{d\bar{\lambda}_{s123}}{dt} \quad (2.7)$$

where R_s is the stator resistance, $\bar{i}_{s123} = (\bar{i}_{s1}, \bar{i}_{s2}, \bar{i}_{s3})^T$ is the stator current vector, $\bar{\lambda}_{s123} = (\bar{\lambda}_{s1}, \bar{\lambda}_{s2}, \bar{\lambda}_{s3})^T$ is the stator flux linkage vector and

$\bar{v}_{s123} = (\bar{v}_{s1}, \bar{v}_{s2}, \bar{v}_{s3})^T$ is the stator voltage vector. All vectors are defined in 123 coordinates.

The superscript T indicates the transposed vector.

The rotor voltage equations are the following:

$$\bar{v}_{r123} = R_r \cdot \bar{i}_{r123} + \frac{d\bar{\lambda}_{r123}}{dt} \quad (2.8)$$

where R_r is the rotor resistance, $\bar{i}_{r123} = (\bar{i}_{r1}, \bar{i}_{r2}, \bar{i}_{r3})^T$ is the rotor current vector and $\bar{\lambda}_{r123} =$

$(\bar{\lambda}_{r1}, \bar{\lambda}_{r2}, \bar{\lambda}_{r3})^T$ is the rotor flux linkage vector. The $\bar{v}_{r123} = (\bar{v}_{r1}, \bar{v}_{r2}, \bar{v}_{r3})^T$ is the rotor voltage vector. Since the motor is a squirrel cage, it has an amplitude equal to zero, indeed it is $\bar{v}_{r123} = (0, 0, 0)^T$.

The equation of the flux linkage of the stator and rotor windings can be written:

$$\bar{\lambda}_{s123} = L_{ls} \cdot \bar{i}_{s123} + M_{123}^{ss} \cdot \bar{i}_{s123} + M_{123}^{sr} \cdot \bar{i}_{r123} \quad (2.9)$$

$$\bar{\lambda}_{r123} = L_{lr} \cdot \bar{i}_{r123} + M_{123}^{rs} \cdot \bar{i}_{s123} + M_{123}^{rr} \cdot \bar{i}_{r123} \quad (2.10)$$

The matrix of the M_{123}^{ss} and M_{123}^{rr} , winding inductances, are:

$$\mathbf{M}_{123}^{ss} = M \cdot \begin{bmatrix} 1 & -\frac{1}{2} & -\frac{1}{2} \\ -\frac{1}{2} & 1 & -\frac{1}{2} \\ -\frac{1}{2} & -\frac{1}{2} & 1 \end{bmatrix}; \mathbf{M}_{123}^{rr} = M \cdot \begin{bmatrix} 1 & -\frac{1}{2} & -\frac{1}{2} \\ -\frac{1}{2} & 1 & -\frac{1}{2} \\ -\frac{1}{2} & -\frac{1}{2} & 1 \end{bmatrix} \quad (2.11)$$

M is the mutual inductance, L_{ls} and L_{lr} are the stator and rotor leakage inductances. M can be considered equal for both stator and rotor windings.

M_{123}^{sr} and M_{123}^{rs} depend on the rotor angle, so these can be written as:

$$\mathbf{M}_{123}^{sr} = [M_{123}^{rs}]^T = M \cdot \begin{bmatrix} \cos(\theta_r) & \cos(\theta_r + \frac{2\pi}{3}) & \cos(\theta_r - \frac{2\pi}{3}) \\ \cos(\theta_r - \frac{2\pi}{3}) & \cos(\theta_r) & \cos(\theta_r + \frac{2\pi}{3}) \\ \cos(\theta_r + \frac{2\pi}{3}) & \cos(\theta_r - \frac{2\pi}{3}) & \cos(\theta_r) \end{bmatrix} \quad (2.12)$$

M is the magnetizing inductance and it can be defined as:

$$M = \frac{N \cdot N'}{\mathfrak{R}_t} \quad (2.13)$$

where N and N' are the number of the equivalent turns and \mathfrak{R}_t is the air gap reluctance.

To facilitate the machine model, mathematical transformations are used:

- Clarke transformation (123 to $\alpha\beta$);
- Park transformation ($\alpha\beta$ to dq).

These transformations are used to simplify the machine model.

2.3 Mathematical model in stationary reference frame ($\alpha\beta$)

A two-phase equivalent machine is considered. In this case, the machine is characterized by two couple of orthogonal windings, one for the stator and the other for the rotor. In Figure 2.3 is shown a sketch of the machine.

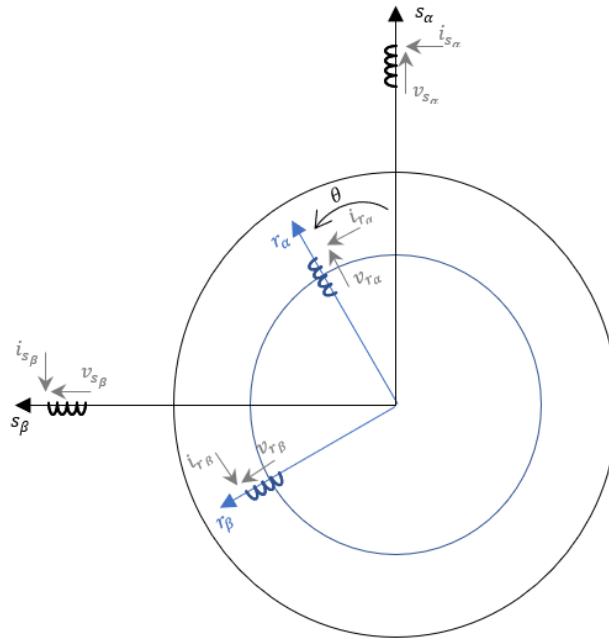


Figure 2.3: Machine model in stationary reference frame ($\alpha\beta$).

The new model ($\alpha\beta$) of the IM is obtained with the Clarke transformation, as shown in

the matrix for a generic one x :

$$\begin{bmatrix} \mathbf{x}_\alpha \\ x_\beta \\ x_0 \end{bmatrix} = [C] \cdot \begin{bmatrix} \mathbf{x}_1 \\ x_2 \\ x_3 \end{bmatrix} = \frac{2}{3} \begin{bmatrix} 1 & -\frac{1}{2} & -\frac{1}{2} \\ 0 & \frac{\sqrt{3}}{2} & -\frac{\sqrt{3}}{2} \\ 1 & 1 & 1 \end{bmatrix} \cdot \begin{bmatrix} \mathbf{x}_1 \\ x_2 \\ x_3 \end{bmatrix} \quad (2.14)$$

The coefficient in front of the matrix defines the properties of the transformation. If it is $\sqrt{\frac{2}{3}}$ the machine power is kept invariant. If it is $\frac{2}{3}$, as in (1.14), the amplitude of the machine is kept invariant.

In this work the coefficient $\frac{2}{3}$ is used. Through the (1.14), the stator and rotor electrical equations are evaluated:

$$\begin{aligned} [C] \cdot \bar{v}_{s123} &= [C] \cdot R_s \cdot \bar{i}_{s123} + [C] \cdot \frac{d\bar{\lambda}_{s123}}{dt} \rightarrow \\ &\rightarrow \bar{v}_{s\alpha\beta 0} = R_s \cdot [C] \cdot \bar{i}_{s123} + \frac{d([C] \cdot \bar{\lambda}_{s123})}{dt} \end{aligned} \quad (2.15)$$

$$\begin{aligned} [C] \cdot \bar{v}_{r123} &= [C] \cdot R_r \cdot \bar{i}_{r123} + [C] \cdot \frac{d\bar{\lambda}_{r123}}{dt} \rightarrow \\ &\rightarrow \bar{v}_{r\alpha\beta 0}^s = R_r \cdot [C] \cdot \bar{i}_{r123} + \frac{d([C] \cdot \bar{\lambda}_{r123})}{dt} \end{aligned} \quad (2.16)$$

The (1.15) and (1.16) can be written in the following ways:

$$\bar{v}_{s\alpha\beta 0} = R_s \cdot \bar{i}_{s\alpha\beta 0} + \frac{d\bar{\lambda}_{s\alpha\beta 0}}{dt} \quad (2.17)$$

$$\bar{v}_{r\alpha\beta 0} = R_r \cdot \bar{i}_{r\alpha\beta 0} + \frac{d\bar{\lambda}_{r\alpha\beta 0}}{dt} \quad (2.18)$$

Through mathematical manipulations is possible to find the flux linkage equations in the

new frame ($\alpha\beta$):

$$\begin{aligned}
 [C] \cdot \bar{\lambda}_{s123} &= [C] \cdot L_{ls} \cdot \bar{i}_{s123} + [C] \cdot M_{123}^{ss} \cdot \bar{i}_{s123} + [C] \cdot M_{123}^{sr} \cdot \bar{i}_{r123} \rightarrow \\
 [C] \cdot \bar{\lambda}_{s123} &= L_{ls} \cdot ([C] \cdot \bar{i}_{s123}) + [C] \cdot M_{123}^{ss} \cdot [C]^{-1} \cdot ([C] \cdot \bar{i}_{s123}) + \\
 &\quad + [C] \cdot M_{123}^{sr} \cdot [C]^{-1} \cdot ([C] \cdot \bar{i}_{r123}) \quad (2.19)
 \end{aligned}$$

$$\begin{aligned}
 [C] \cdot \bar{\lambda}_{r123} &= [C] \cdot L_{lr} \cdot \bar{i}_{r123} + [C] \cdot M_{123}^{rs} \cdot \bar{i}_{s123} + [C] \cdot M_{123}^{rr} \cdot \bar{i}_{r123} \rightarrow \\
 [C] \cdot \bar{\lambda}_{r123} &= L_{lr} \cdot ([C] \cdot \bar{i}_{r123}) + [C] \cdot M_{123}^{rs} \cdot [C]^{-1} \cdot ([C] \cdot \bar{i}_{s123}) + \\
 &\quad + [C] \cdot M_{123}^{rr} \cdot [C]^{-1} \cdot ([C] \cdot \bar{i}_{r123}) \quad (2.20)
 \end{aligned}$$

Thought the (1.19) and (1.20), the magnetic equations can be written as:

$$\bar{\lambda}_{s\alpha\beta 0} = L_{ls} \cdot \bar{i}_{s\alpha\beta 0} + M_{\alpha\beta 0}^{ss} \cdot \bar{i}_{s\alpha\beta 0} + M_{\alpha\beta 0}^{sr} \cdot \bar{i}_{r\alpha\beta 0} \quad (2.21)$$

$$\bar{\lambda}_{r\alpha\beta 0} = L_{lr} \cdot \bar{i}_{r\alpha\beta 0} + M_{\alpha\beta 0}^{rs} \cdot \bar{i}_{s\alpha\beta 0} + M_{\alpha\beta 0}^{rr} \cdot \bar{i}_{r\alpha\beta 0} \quad (2.22)$$

The new matrices are defined as:

$$\begin{aligned}
 M_{\alpha\beta 0}^{ss} &= [C] \cdot M_{123}^{ss} \cdot [C]^{-1} & M_{\alpha\beta 0}^{sr} &= [C] \cdot M_{123}^{sr} \cdot [C]^{-1} \\
 M_{\alpha\beta 0}^{rs} &= [C] \cdot M_{123}^{rs} \cdot [C]^{-1} & M_{\alpha\beta 0}^{rr} &= [C] \cdot M_{123}^{rr} \cdot [C]^{-1}
 \end{aligned} \quad (2.23)$$

and they are characterized by the following properties:

$$M_{\alpha\beta 0}^{ss} = M_{\alpha\beta 0}^{rr} \quad (2.24)$$

$$M_{\alpha\beta 0}^{rs} = (M_{\alpha\beta 0}^{sr})^T \quad (2.25)$$

They can be define in this form:

$$\mathbf{M}_{\alpha\beta 0}^{ss} = M_{\alpha\beta 0}^{rr} = \frac{3}{2} \cdot M \cdot \begin{bmatrix} 1 & 0 & 0 \\ 0 & 1 & 0 \\ 0 & 0 & 0 \end{bmatrix} \quad (2.26)$$

$$\mathbf{M}_{\alpha\beta 0}^{sr} = (M_{\alpha\beta 0}^{rs})^T = \frac{3}{2} \cdot M \cdot \begin{bmatrix} \cos \theta & \sin \theta & 0 \\ -\sin \theta & \cos \theta & 0 \\ 0 & 0 & 0 \end{bmatrix} \quad (2.27)$$

The equations can be rewritten in a compact form. In this way can obtain the electromagnetic equations:

$$\begin{cases} \bar{v}_{s\alpha\beta 0} = R_s \cdot \bar{i}_{s\alpha\beta 0} + \frac{d\lambda_{s\alpha\beta 0}}{dt} \\ \bar{v}_{r\alpha\beta 0} = R_r \cdot \bar{i}_{r\alpha\beta 0} + \frac{d\lambda_{r\alpha\beta 0}}{dt} \end{cases} \quad (2.28)$$

$$\begin{cases} \bar{\lambda}_{s\alpha\beta 0} = L_{ls} \cdot \bar{i}_{s\alpha\beta 0} + M_{\alpha\beta 0}^{ss} \cdot \bar{i}_{s\alpha\beta 0} + M_{\alpha\beta 0}^{sr} \cdot \bar{i}_{r\alpha\beta 0} \\ \bar{\lambda}_{r\alpha\beta 0} = L_{lr} \cdot \bar{i}_{r\alpha\beta 0} + M_{\alpha\beta 0}^{rs} \cdot \bar{i}_{s\alpha\beta 0} + M_{\alpha\beta 0}^{rr} \cdot \bar{i}_{r\alpha\beta 0} \end{cases}$$

The components 0 are decoupled from the $(\alpha\beta)$ axes as follows:

$$\begin{cases} \bar{v}_{s0} = R_s \cdot \bar{i}_{s0} + \frac{d\lambda_{s0}}{dt} \\ \bar{v}_{r0} = R_r \cdot \bar{i}_{r0} + \frac{d\lambda_{r0}}{dt} \end{cases} \rightarrow \begin{cases} \bar{\lambda}_{s0} = L_{ls} \cdot \bar{i}_{s0} \\ \bar{\lambda}_{r0} = L_{lr} \cdot \bar{i}_{r0} \end{cases} \quad (2.29)$$

$$\rightarrow \begin{cases} \bar{v}_{s0} = R_s \cdot \bar{i}_{s0} + L_{ls} \cdot \frac{di_{s0}}{dt} \\ \bar{v}_{r0} = R_r \cdot \bar{i}_{r0} + L_{lr} \cdot \frac{di_{r0}}{dt} \end{cases}$$

The $(\alpha\beta)$ frame is also called "stationary frame".

2.4 Mathematical model in rotating reference frame (dq)

The inductance matrices in (2.26) and (2.27) depend on the angle θ . The latter is the electric angle and thanks to it it is possible to calculate the position of the rotor. The rotating

reference frame is used for the control of the machine.

The electromagnetic model is a generic reference frame, with a rotation ω_k . The speed ω_k is computed using the rotational matrix shown in (2.30):

$$\mathbf{R}(\theta_k) = \begin{bmatrix} \cos(\theta_k) & -\sin(\theta_k) \\ \sin(\theta_k) & \cos(\theta_k) \end{bmatrix} \quad (2.30)$$

where θ_k is the angle of the frame, leading to as follows:

$$\omega_k = \frac{d(\theta_k)}{dt} \quad (2.31)$$

Equations (2.28) have been taken into account. These equations represent the stator and rotor equations in a stationary frame. The rotation (2.30) was applied only to the components $(\alpha\beta)$.

In this way, we get the following:

$$\begin{cases} [R(\theta_k)] \cdot \bar{v}_{s\alpha\beta 0} = [R(\theta_k)] \cdot R_s \cdot \bar{i}_{s\alpha\beta 0} + [R(\theta_k)] \cdot \frac{d\lambda_{s\alpha\beta 0}}{dt} \\ [R(\theta_k)] \cdot \bar{v}_{r\alpha\beta 0} = [R(\theta_k)] \cdot R_r \cdot \bar{i}_{r\alpha\beta 0} + [R(\theta_k)] \cdot \frac{d\lambda_{r\alpha\beta 0}}{dt} \end{cases} \quad (2.32)$$

$$\begin{cases} [R(\theta_k)] \cdot \bar{\lambda}_{s\alpha\beta 0} = [R(\theta_k)] \cdot L_{ls} \cdot \bar{i}_{s\alpha\beta 0} + [R(\theta_k)] \cdot M_{\alpha\beta 0}^{ss} \cdot \bar{i}_{s\alpha\beta 0} + [R(\theta_k)] \cdot M_{\alpha\beta 0}^{sr} \cdot \bar{i}_{r\alpha\beta 0} \\ [R(\theta_k)] \cdot \bar{\lambda}_{r\alpha\beta 0} = [R(\theta_k)] \cdot L_{lr} \cdot \bar{i}_{r\alpha\beta 0} + [R(\theta_k)] \cdot M_{\alpha\beta 0}^{rs} \cdot \bar{i}_{s\alpha\beta 0} + [R(\theta_k)] \cdot M_{\alpha\beta 0}^{rr} \cdot \bar{i}_{r\alpha\beta 0} \end{cases}$$

The rotor position depends on the time, for this reason, the rotational cannot be included in the time derivative. therefore, the following artifice is performed:

$$\begin{bmatrix} f_{k1} \\ f_{k2} \end{bmatrix} = [R(\theta_k)] \cdot \begin{bmatrix} f_\alpha \\ f_\beta \end{bmatrix} \rightarrow \begin{bmatrix} f_\alpha \\ f_\beta \end{bmatrix} = [R(\theta_k)]^{-1} \cdot \begin{bmatrix} f_{k1} \\ f_{k2} \end{bmatrix} \quad (2.33)$$

As a result of the (2.32). It is possible to write:

$$\begin{cases} \bar{v}_{sk} = R_s \cdot \bar{i}_{sk} + [R(\theta_k)] \cdot \frac{d([R(\theta_k)]^{-1} \cdot \bar{\lambda}_{sk})}{dt} \\ \bar{v}_{rk} = R_r \cdot \bar{i}_{rk} + [R(\theta_k)] \cdot \frac{d([R(\theta_k)]^{-1} \cdot \bar{\lambda}_{rk})}{dt} \end{cases} \quad (2.34)$$

$$\begin{cases} \bar{\lambda}_{sk} = L_{ls} \cdot \bar{i}_{sk} + [R(\theta_k)] \cdot M^{sr} \cdot ([R(\theta_k)]^{-1} \cdot \bar{i}_{rk}) + M^{ss} \cdot \bar{i}_{sk} \\ \bar{\lambda}_{rk} = L_{lr} \cdot \bar{i}_{rk} + [R(\theta_k)] \cdot M^{rs} \cdot ([R(\theta_k)]^{-1} \cdot \bar{i}_{sk}) + M^{rr} \cdot \bar{i}_{rk} \end{cases}$$

The product between the inductances matrices ($M^{ss}, M^{rr}, M^{sr}, M^{rs}$), the rotational matrix $R(\theta_k)$ and its inverse, take the following form:

$$M^{ss} = M^{rr} = M^{sr} = M^{rs} = \frac{3}{2} \cdot M \cdot \begin{bmatrix} 1 & 0 \\ 0 & 1 \end{bmatrix} \quad (2.35)$$

After performing mathematical manipulations, the equations in a generic reference frame can be written as follows:

$$\begin{cases} \bar{v}_s = R_s \cdot \bar{i}_s + \frac{d\bar{\lambda}_s}{dt} + j \cdot \omega_k \cdot \bar{\lambda}_s \\ \bar{v}_r = R_r \cdot \bar{i}_r + \frac{d\bar{\lambda}_r}{dt} + j \cdot (\omega_k - \omega_r) \cdot \bar{\lambda}_r \end{cases} \quad (2.36)$$

$$\begin{cases} \bar{\lambda}_s = L_s \cdot \bar{i}_s + L_m \cdot \bar{i}_r, & L_s = L_{ls} + L_m, & L_m = \frac{3}{2} \cdot M \\ \bar{\lambda}_r = L_m \cdot \bar{i}_s + L_r \cdot \bar{i}_r, & L_r = L_{lr} + L_m, & L_m = \frac{3}{2} \cdot M \end{cases}$$

where L_m is the magnetizing inductance and the $\frac{3}{2}$ is the coefficient of the Clarke transformation.

To evaluate the torque equation, we needed to start of the balance of the powers. The equation of the electrical power is the follows:

$$P_e = \bar{v}_s \cdot \bar{i}_s + \bar{v}_r \cdot \bar{i}_r = P_{Jsr} + P_m + P_{me} \rightarrow$$

$$\rightarrow \begin{cases} \bar{v}_s \cdot \bar{i}_s = R_s \cdot |\bar{i}_s|^2 + \frac{d\bar{\lambda}_s}{dt} \cdot \bar{i}_s + j \cdot \omega_k \cdot \bar{\lambda}_s \cdot \bar{i}_s \\ 0 = \bar{v}_r \cdot \bar{i}_r = R_r \cdot |\bar{i}_r|^2 + \frac{d\bar{\lambda}_r}{dt} \cdot \bar{i}_r + j \cdot (\omega_k - \omega_r) \cdot \bar{\lambda}_r \cdot \bar{i}_r \end{cases} \quad (2.37)$$

where P_{Jsr} is the Joule power, P_m is the magnetizing power and P_{em} is the electromagnetic power. These powers are defined in the following way:

$$\begin{aligned} P_{Jsr} &= R_s \cdot |\bar{i}_s|^2 + R_r \cdot |\bar{i}_r|^2 \\ P_m &= \frac{d\bar{\lambda}_s}{dt} \cdot \bar{i}_s + \frac{d\bar{\lambda}_r}{dt} \cdot \bar{i}_r \\ P_{em} &= (j \cdot \omega_k \cdot \bar{\lambda}_s) \cdot \bar{i}_s + (j \cdot \omega_k \cdot \bar{\lambda}_r) \cdot \bar{i}_r - (j \cdot \omega_r \cdot \bar{\lambda}_r) \cdot \bar{i}_r \end{aligned} \quad (2.38)$$

The P_{em} does not depend on the chosen reference frame. For this reason, it becomes:

$$P_{em} = -(j \cdot \omega_r \cdot \bar{\lambda}_r) \cdot \bar{i}_r = \omega_r \cdot (\bar{i}_r \wedge \bar{\lambda}_r) \quad (2.39)$$

The torque equation can be written:

$$T_{em} = \frac{3}{2} \cdot pp \cdot (\bar{i}_r \wedge \bar{\lambda}_r) \quad (2.40)$$

where pp is the number of pole pairs and $\frac{3}{2}$ is the coefficient of the Clarke transformation.

By combining (2.36) with (2.40), the electromagnetic torque can be expressed as:

$$T_{em} = \frac{3}{2} \cdot pp \cdot (\bar{i}_r \wedge M \cdot \bar{i}_s) = \frac{3}{2} \cdot pp \cdot (\bar{\lambda}_s \wedge \bar{i}_s) \quad (2.41)$$

2.5 Equivalent circuit in rotating coordinates

In this section, the equivalent circuit of the machine in rotating coordinates is provided.

Starting from (2.36):

- $\omega_k = \omega_s$: this means that synchronous speed is equal to the pulsation of the supply voltage;
- all the time-derivatives are equal to zero; in this case, the steady-state condition is provided.

Hence, the electromagnetic equations can be written in rotating dq coordinates:

$$\begin{cases} \bar{V}_{sdq} = R_s \cdot \bar{I}_{sdq} + j \cdot \omega_e \cdot \bar{\Lambda}_{sdq} \\ \bar{V}_{rdq} = R_r \cdot \bar{I}_{rdq} + j \cdot (\omega_e - \omega_r) \cdot \bar{\Lambda}_{rdq} \end{cases} \quad (2.42)$$

$$\rightarrow \begin{cases} \bar{\Lambda}_{sdq} = L_s \cdot \bar{I}_{sdq} + L_m \cdot \bar{I}_{rdq} \\ \bar{\Lambda}_{rdq} = L_m \cdot \bar{I}_{sdq} + L_r \cdot \bar{I}_{rdq} \end{cases}$$

If the electrical equations are substituted in the magnetic ones, it is possible to obtain the electromagnetic equations:

$$\begin{cases} \bar{V}_{sdq} = R_s \cdot \bar{I}_{sdq} + j \cdot \omega_e \cdot L_s \cdot \bar{I}_{sdq} + j \cdot \omega_e \cdot M \cdot \bar{I}_{rdq} \\ 0 = \frac{R_r}{s} \cdot \bar{I}_{rdq} + j \cdot \omega_e \cdot L_r \cdot \bar{I}_{rdq} + j \cdot \omega_e \cdot M \cdot \bar{I}_{sdq} \end{cases} \quad (2.43)$$

$$\rightarrow \begin{cases} \bar{V}_{sdq} = (R_s + j \cdot \omega_e \cdot L_s) \cdot \bar{I}_{sdq} + j \cdot \omega_e \cdot M \cdot \bar{I}_{rdq} \\ 0 = (\frac{R_r}{s} + j \cdot \omega_e \cdot L_r) \cdot \bar{I}_{rdq} + j \cdot \omega_e \cdot M \cdot \bar{I}_{sdq} \end{cases}$$

Starting from the (2.4), it is possible to sketch the equivalent circuit of the machine in rotation dq coordinates. It is shown in Figure 2.4:

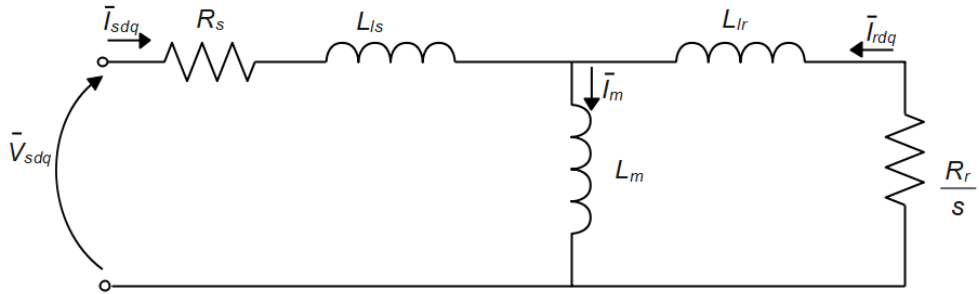


Figure 2.4: Equivalent circuit in the (dq) rotor reference frame.

The position of the rotor flux vector is considered the d -axis, so the magnetic equations in dq coordinates are the follows:

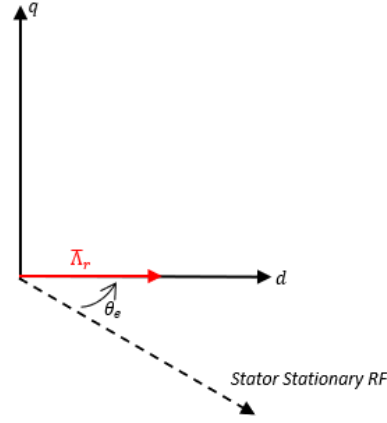


Figure 2.5: Rotor flux vector in (dq) coordinates.

$$\begin{cases} \Lambda_r = M \cdot I_{sd} \\ (\omega_e - \omega_r) \cdot \tau_r \cdot \Lambda_r = M \cdot I_{sq} \end{cases} \quad (2.44)$$

Considering (2.44), the equation of the electromagnetic torque can be written:

$$T_{em} = \frac{3}{2} \cdot pp \cdot k_r \cdot \Lambda_r \cdot I_{sq} \quad (2.45)$$

where k_r is the rotor coupling coefficient, defined in (2.46), and it is used to define the flux weakening of the machine:

$$k_r = \frac{L_m}{L_r} \quad (2.46)$$

In steady-state conditions, based on (2.44), the slip speed is:

$$\omega_{sl} = \frac{I_{sq}}{\tau_r \cdot I_{sd}} \quad (2.47)$$

Starting on (2.44), the vector of the rotor currents is computed:

$$\bar{I}_r = \frac{\bar{\Lambda}_r - M \cdot \bar{I}_s}{L_r} \rightarrow \begin{cases} I_{rd} = \frac{\Lambda_r - M \cdot \bar{I}_{sd}}{L_r} = 0 \\ I_{rq} = \frac{-M \cdot \bar{I}_{sq}}{L_r} = -k_r \cdot I_{sq} \end{cases} \quad (2.48)$$

In steady-state conditions, the rotor current is composed only of the flux component in the q -axis. The current vectors are shown in Figure 2.6. The current \bar{I}_m is the vector of the magnetizing current and is the sum of those of the stator and rotor.

Using (2.42), the magnetizing flux can be highlighted in the magnetic equations as:

$$\begin{cases} \bar{\Lambda}_{sdq} = L_{ls} \cdot \bar{I}_{sdq} + L_m \cdot \bar{I}_m \\ \bar{\Lambda}_{rdq} = L_{lr} \cdot \bar{I}_{rdq} + L_m \cdot \bar{I}_m \end{cases} \quad (2.49)$$

After mathematical manipulations, the (dq) inductances of the machine can be computed as in (2.50):

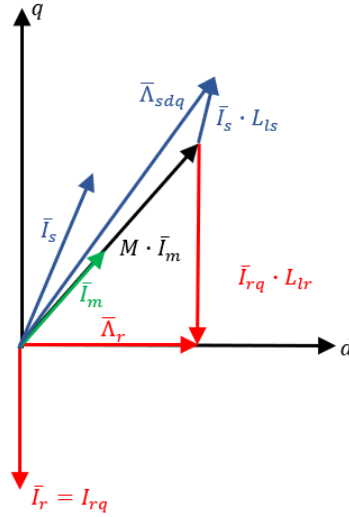


Figure 2.6: Stator and Rotor current vectors in (dq) coordinates (steady-state conditions).

$$\begin{cases} \Lambda_{sd} = \Lambda_r + L_{ls} \cdot I_{sd} = M \cdot I_{sd} + L_{ls} \cdot I_{sd} = (L_{ls} + M) \cdot I_{sd} \\ \Lambda_{sq} = L_{ls} \cdot I_{sq} + k_r \cdot L_{lr} \cdot I_{sq} = (L_{ls} + k_r \cdot L_{lr}) \cdot I_{sq} \end{cases} \quad (2.50)$$

$$\rightarrow \begin{cases} \Lambda_{sd} = L_d \cdot I_{sd} \\ \Lambda_{sq} = L_q \cdot I_{sq} \end{cases}$$

The inductance along the q -axis is:

$$\begin{aligned} L_q &= L_{ls} + k_r \cdot L_{lr} = (L_s - M) + k_r \cdot (L_r - M) \\ &\rightarrow L_q = L_s \cdot (1 - k_s \cdot k_r) = \sigma \cdot L_s \end{aligned} \quad (2.51)$$

where σ is the overall decoupling coefficient.

2.6 Induction machine model

In this section, the induction motor model will be shaped.

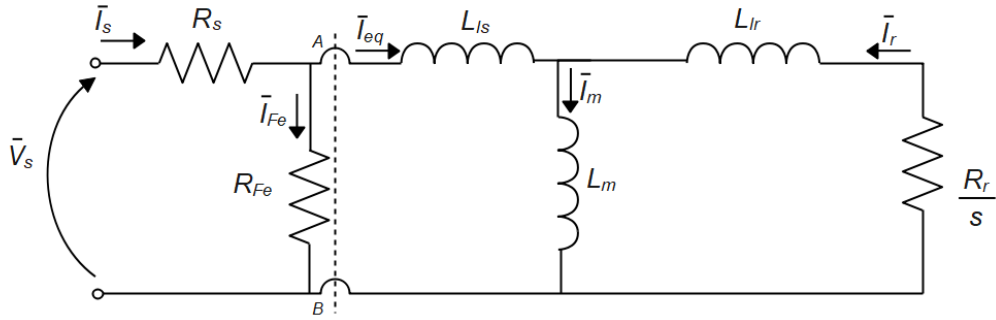


Figure 2.7: Equivalent circuit in (dq) reference frame.

In steady-state conditions, the electromagnetic equations in the (dq) reference frame are:

$$\begin{cases} \bar{V}_s = R_s \cdot \bar{I}_s + j \cdot \omega_e \cdot \bar{\Lambda}_s \\ \bar{0} = -R_{Fe} \cdot \bar{I}_{Fe} + j \cdot \omega_e \cdot \bar{\Lambda}_s \\ \bar{0} = \frac{R_r}{s} \cdot \bar{I}_r + j \cdot (\omega_e - \omega_r) \cdot \bar{\Lambda}_r \end{cases} \quad \begin{cases} \bar{\Lambda}_s = L_{ls} \cdot (\bar{I}_s - \bar{I}_{Fe}) + L_m \cdot (\bar{I}_s - \bar{I}_{Fe} + \bar{I}_r) \\ \bar{\Lambda}_r = L_{lr} \cdot \bar{I}_r + L_m \cdot (\bar{I}_s - \bar{I}_{Fe} + \bar{I}_r) \end{cases} \quad (2.52)$$

By introducing the slip and by substituting the magnetic equations in the electrical equations, the (2.52) can be written as follows:

$$\begin{cases} \bar{V}_s = R_s \cdot \bar{I}_s + j \cdot \omega_e \cdot L_{ls} \cdot (\bar{I}_s - \bar{I}_{Fe}) + j \cdot \omega_e \cdot L_m \cdot (\bar{I}_s - \bar{I}_{Fe} + \bar{I}_r) \\ \bar{0} = -R_{Fe} \cdot \bar{I}_{Fe} + j \cdot \omega_e \cdot L_{ls} \cdot (\bar{I}_s - \bar{I}_{Fe}) + j \cdot \omega_e \cdot L_m \cdot (\bar{I}_s - \bar{I}_{Fe} + \bar{I}_r) \\ \bar{0} = \frac{R_r}{s} \cdot \bar{I}_r + j \cdot (\omega_e - \omega_r) \cdot L_{lr} \cdot \bar{I}_r + j \cdot (\omega_e - \omega_r) \cdot L_m \cdot (\bar{I}_s - \bar{I}_{Fe} + \bar{I}_r) \end{cases} \quad (2.53)$$

To simplify the model, we can apply the equivalent Thevenin circuit that runs to the AB terminals and introduce an equivalent voltage V_{eq} , an equivalent resistance R_{eq} and an equivalent current I_{eq} . These quantities can be written as:

$$R_{eq} = \frac{R_s \cdot R_{Fe}}{R_s + R_{Fe}}; \quad \bar{V}_{eq} = \bar{V}_s \cdot \frac{R_{Fe}}{R_s + R_{Fe}}; \quad \bar{I}_{eq} = \bar{I}_s - \bar{I}_{Fe} \quad (2.54)$$

According to the equivalent circuit shown in Figure 1.6, the equations become:

$$\begin{cases} \bar{V}_{eq} = R_{eq} \cdot \bar{I}_{eq} + j \cdot \omega_e \cdot \Lambda_s \\ \bar{0} = \frac{R_r}{s} \cdot \bar{I}_r + j \cdot (\omega_e - \omega_r) \cdot \bar{\Lambda}_r \end{cases} \quad \begin{cases} \bar{\Lambda}_s = L_s \cdot \bar{I}_{eq} + L_m \cdot \bar{I}_r \\ \bar{\Lambda}_r = L_r \cdot \bar{I}_r + L_m \cdot \bar{I}_{eq} \end{cases} \quad (2.55)$$

2.7 Test of induction machine

To evaluate the induction motor parameters, it is necessary to carry out the No-Load test and the Locked-rotor Test. With the first test, it is possible to find the resistance that model the iron losses R_{Fe} , the magnetizing inductance L_m , the iron I_{Fe} and magnetization I_m currents.

With the second test, the rotor resistance R_r , the stator L_s and the rotor r inductances are calculated.

2.7.1 No-load test

The no-load test is conducted with a set frequency and with different voltage values, so it is possible to evaluate the magnetic saturation law. If the test is performed at different frequencies, the iron losses model is obtained. In this case, the slip is equal to 0

The equivalent circuit of the no-load test is shown in Figure 2.8:

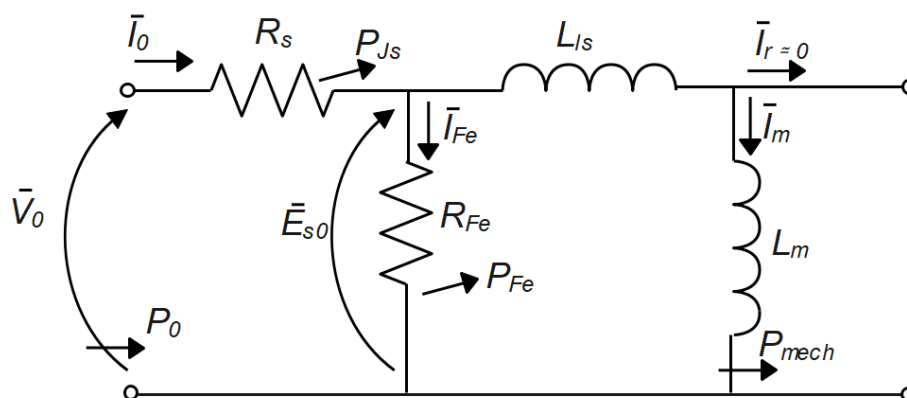


Figure 2.8: Equivalent circuit of the no-load test.

P_0 , V_0 and I_0 are respectively the input power, voltage and current related to the no-load circuit. Initially, the test is performed with low voltage values, so it is possible to divide the mechanical losses from those of the iron. The sum of the mechanical and iron losses can be estimated by subtracting the stator Joule losses P_{Js} and the input power P_0 .

$$P_{mech+Fe} = P_0 - 3 \cdot R_s \cdot I_0^2 \quad (2.56)$$

The iron losses can be neglected with low voltage values, so the (2.56) corresponds to the mechanical power. With different frequency values, the mechanical power can be written according to the machine speed. Furthermore, the mechanical power corresponds to the torque loss that must be subtracted to that electromagnetic (2.45) in motoring mode and vice versa in generating mode. In general, the mechanical losses are linked with the friction and ventilation.

To search the parameters of the machine, it is necessary to start from the voltage E_{s0} , as shown below:

$$E_{s0} = \sqrt{(V_0 - R_s \cdot \cos(\phi_0) \cdot I_0)^2 + (R_s \cdot \sin(\phi_0) \cdot I_0)^2}, \quad \cos(\phi_0) = \frac{P_0}{3 \cdot V_0 \cdot I_0} \quad (2.57)$$

To conclude, the parameters are calculated as follows:

$$R_{Fe} = 3 \cdot \frac{E_{s0}^2}{P_{Fe}}; \quad I_{Fe} = \frac{E_{s0}^2}{R_{Fe}}; \quad I_m = \sqrt{I_0^2 - I_{Fe}^2}; \quad X_s = X_m + X_{ls} = \frac{E_{s0}}{I_m} \quad (2.58)$$

X_s is the stator reactance and it is the sum of the magnetizing X_m and leakage X_{ls} reactances.

X_{ls} is evaluated in the next paragraph from the locked-rotor test.

2.7.2 Locked-rotor test

The equivalent circuit of the locked-rotor test is shown in Figure 2.9. In this case the iron resistance and inductance are negligible and the slip is equal to 1.

P_{scc} , V_{scc} and I_{scc} are respectively the input power, voltage and current related to the locked-rotor circuit and they will be calculated in the next equations.

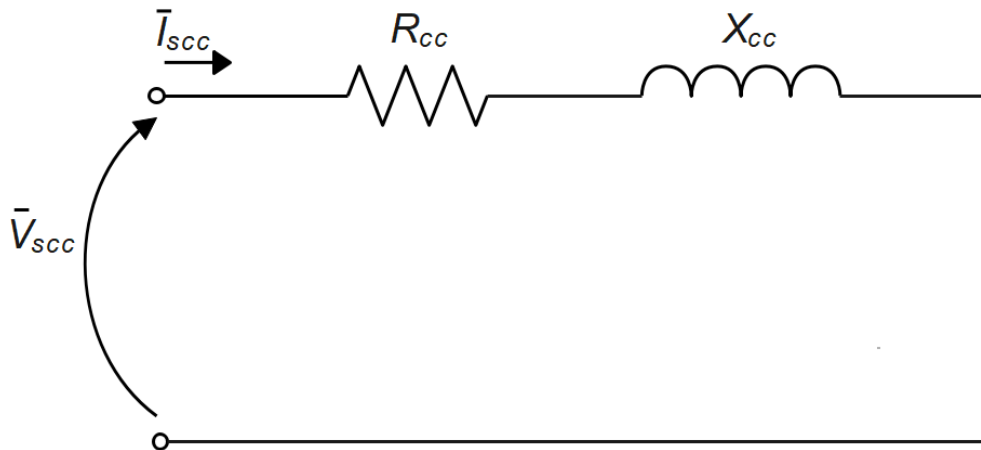


Figure 2.9: Equivalent circuit of the no-load test.

The frequency is imposed, so the parameters can be written as:

$$Q_{cc} = \sqrt{3 \cdot V_{scc}^2 \cdot I_{scc}^2 - P_{scc}^2}; \quad R_{cc} = \frac{P_{scc}}{3 \cdot I_{scc}^2}; \quad X_{cc} = \frac{Q_{cc}}{3 \cdot I_{scc}^2} \quad (2.59)$$

Starting on the (2.58) and (2.59), the machine inductances X_r and X_s are evaluated as:

$$\begin{aligned}
 X_{ls} = X_{lr} &\simeq \frac{X_{cc}}{2} \rightarrow L_{ls} = L_{lr} \simeq \frac{1}{2} \cdot \frac{X_{cc}}{\omega_e} \\
 X_m = X_s - X_{ls} &\rightarrow L_m = \frac{X_m}{\omega_e} \\
 R_r &= R_{cc} - R_s
 \end{aligned}
 \tag{2.60}$$

Finally, the parameters are evaluated.

2.8 Mathematical model of Voltage Source Inverter (VSI)

As a side-activity, the Voltage Source Inverter (VSI) model was studied and developed [5]. This can be useful for future activities related to motor control. The inverter implemented is a 2-Level VSI. In Figure 2.12 is shown the scheme of the inverter;

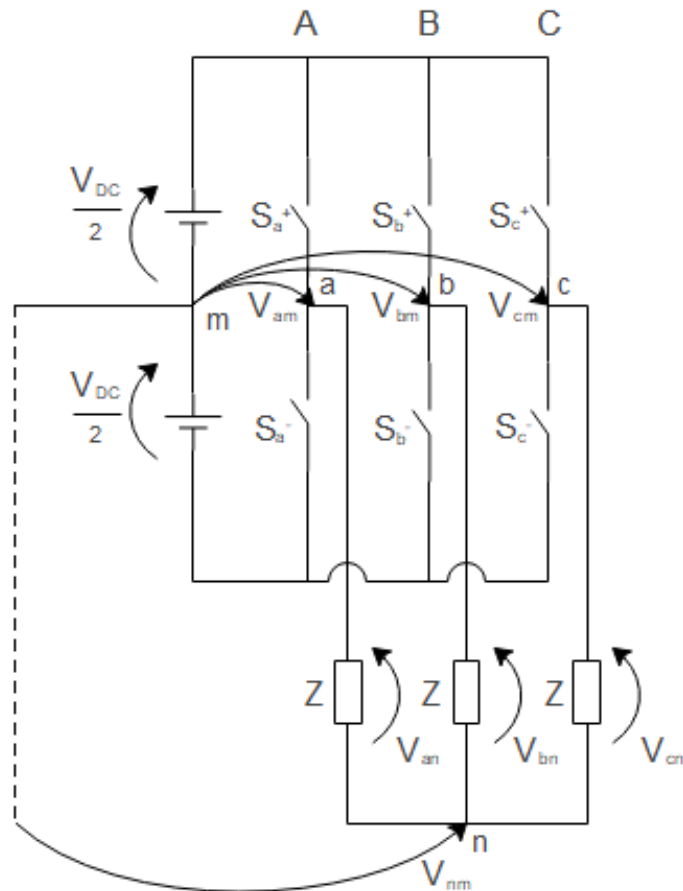


Figure 2.10: Three-phase inverter.

The VSI with ideal switches is connected to a symmetrical and balanced load, this load is without neutral. The load is characterized by an impedance equal to Z .

The inverter shown in Figure 2.12 is made with six switches and it is possible to see three branches A, B, C . These branches can be used to connect two switches in series and these work in a complementary way.

S_a, S_b and S_c are the states of the branches and they can be only +1 or -1. These states represent if and which switches are closed.

The voltage on branches is:

$$V_{am} = S_A \cdot \frac{V_{DC}}{2} \quad (2.61)$$

$$V_{bm} = S_B \cdot \frac{V_{DC}}{2} \quad (2.62)$$

$$V_{cm} = S_C \cdot \frac{V_{DC}}{2} \quad (2.63)$$

The voltage on the load can be expressed as [6]:

$$V_{an} = V_{am} - V_{nm} \quad (2.64)$$

$$V_{bn} = V_{bm} - V_{nm} \quad (2.65)$$

$$V_{cn} = V_{cm} - V_{nm} \quad (2.66)$$

In the reality, the load voltage V_{nm} is not measured because the centre of the load is not accessible, so the (2.64), (2.65) and (2.66) are not calculated and they are only theoretical values. V_{nm} can be calculated as a function of voltages branches and can be written as:

$$V_{an} + V_{bn} + V_{cn} = V_{am} + V_{bm} + V_{cm} - 3 \cdot V_{nm} \quad (2.67)$$

Considering a symmetrical and balanced load without neutral, V_{nm} can be defined by the (2.67) and can be written as follows:

$$V_{an} + V_{bn} + V_{cn} = 0 \rightarrow V_{nm} = \frac{V_{am} + V_{bm} + V_{cm}}{3} \quad (2.68)$$

By the (2.68) is possible to express the equations which describe the phase voltages; the branch voltages are:

$$V_{an} = \frac{2}{3} \cdot V_{am} - \frac{1}{3} \cdot (V_{bm} + V_{cm}) \quad (2.69)$$

$$V_{bn} = \frac{2}{3} \cdot V_{bm} - \frac{1}{3} \cdot (V_{am} + V_{cm}) \quad (2.70)$$

$$V_{cn} = \frac{2}{3} \cdot V_{cm} - \frac{1}{3} \cdot (V_{am} + V_{bm}) \quad (2.71)$$

These equations can be organized in vector form and can be written as:

$$\begin{pmatrix} V_{an} \\ V_{bn} \\ V_{cn} \end{pmatrix} = \frac{V_{DC}}{2} \cdot \begin{pmatrix} \frac{2}{3} & -\frac{1}{3} & -\frac{1}{3} \\ -\frac{1}{3} & \frac{2}{3} & -\frac{1}{3} \\ -\frac{1}{3} & -\frac{1}{3} & \frac{2}{3} \end{pmatrix} \cdot \begin{pmatrix} S_A \\ S_B \\ S_C \end{pmatrix} \quad (2.72)$$

Considering that the leg states are 2 and that the three-phase inverter branches are 3, the number of vectors that can be applied to the load are $2^3=8$; it is shown below:

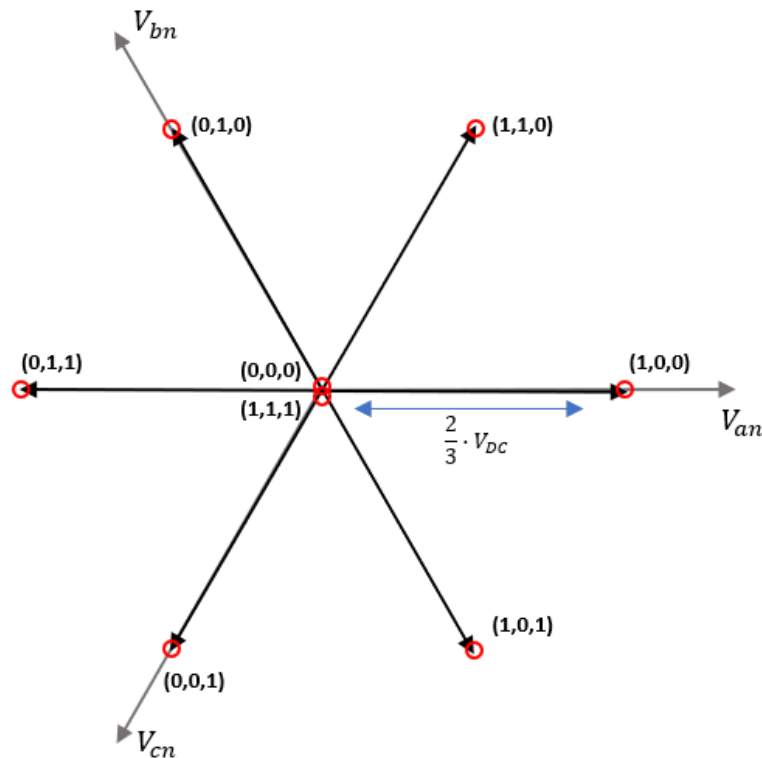


Figure 2.11: Voltage vectors.

The zero voltage vectors correspond to the two state in which the upper and lower

switched of the three branches are closed.

The Figure 2.11 in literature is called *hexagon of the output voltages of the three-phase inverter*.

Since the inverter implementation was a side-activity, this was implemented only in Matlab/Simulink. The Simulink model is shown below:

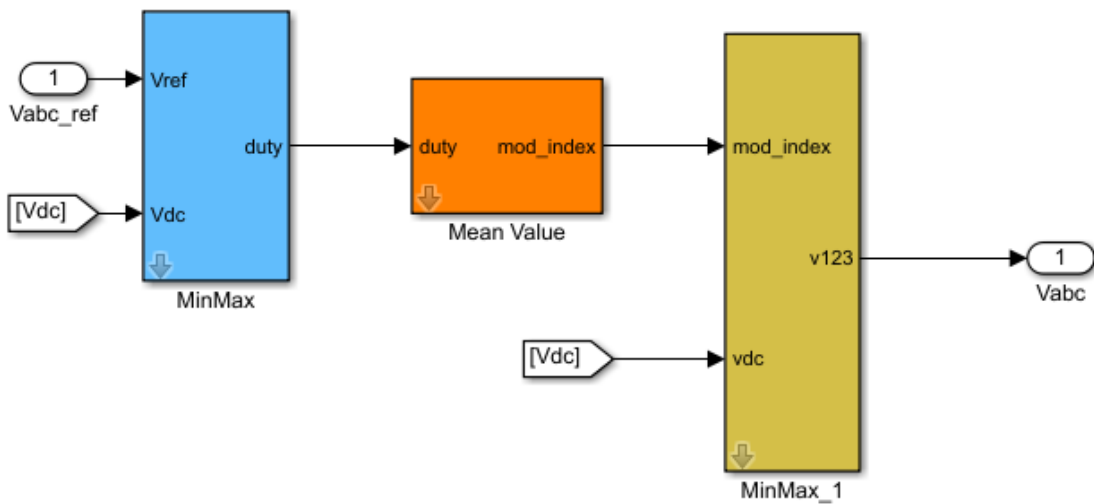


Figure 2.12: Voltage Source Inverter.

In this Simulink model, you can see the V_{ref} , these are three sinusoidal reference voltages, and the V_{dc} which is the common mode voltage. In this case, for example, for simulations, V_{ref} and V_{dc} are considered respectively 220V and 400V. The modulation indices are calculated from the *MinMax* block and are represented as follows:

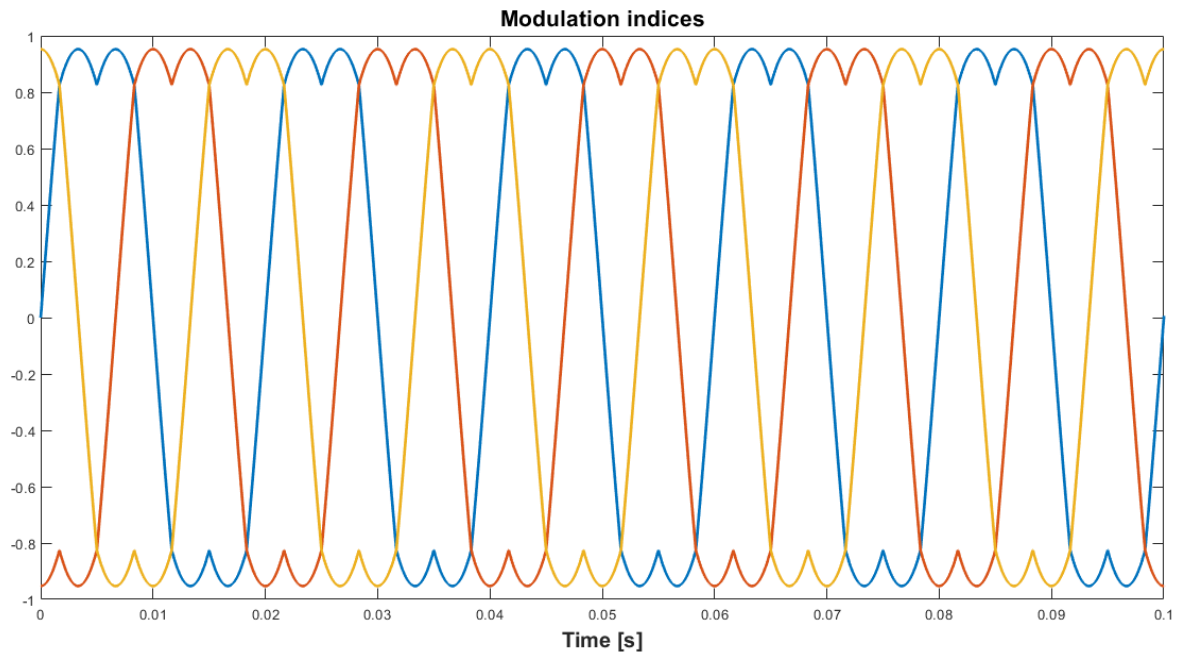


Figure 2.13: Modulation indices.

In the block *MinMax1*, the modulation indices are multiplied by V_{dc} . The output of this block is the three sinusoidal voltages and they are limited in the range:

$$\pm \frac{V_{dc}}{\sqrt{3}}$$

and it is shown in Figure 2.14

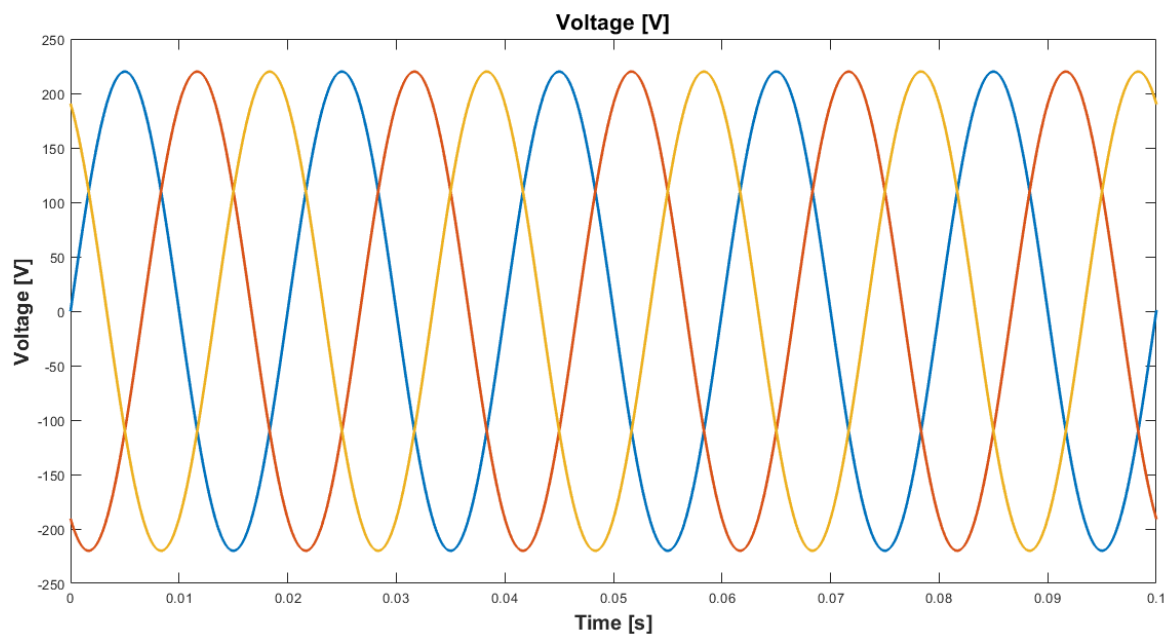


Figure 2.14: Voltage.

Chapter 3

Simulink and dSPACE comparisons in stationary reference frame $(\alpha\beta)$

The purpose of the activity was to implement the Squirrel Cage Induction Motor (SCIM) model in Simulink and dSPACE.

In this chapter, the two models are implemented in $(\alpha\beta)$ coordinates.

The Simulink model used as benchmark for the dSPACE – XSG model was inherited from a model developed in dynamics of electrical machines course of Politecnico di Torino.

In Simulink and dSPACE the three-phase sinusoidal voltage generator, the induction motor and the mechanic were implemented. The simulations were developed in open-loop. Open-loop simulation is obtained by providing a known input and verifying that the outputs are those expected and that they follow the desired behaviour.

First, the development of the Simulink $(\alpha\beta)$ model is analysed and an overview of the model is providing.

After that, a description of dSPACE is given and also in this case an overview of the dSPACE $(\alpha\beta)$ model is provided.

3.1 Overview on Simulink model

Starting from the equations described in Chapter 1, the Simulink model can be modelled. The blocks below represent the simulation scheme adopted for Simulink model.

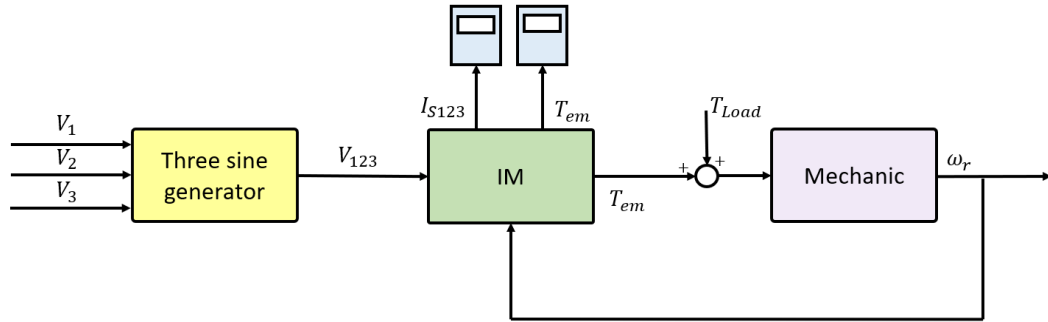


Figure 3.1: Scheme of the model.

In this scheme, three sine waves are used, and thanks to Clarke's transformation, they are transformed into ($\alpha\beta$) coordinates. The Clark transform is a 3x3 matrix. In this case the *Amplitude invariant* is used and can be written as (2.14).

The x_0 component is not involved in conversion and it is called *homopolar component*.

At this point, the voltages are two components and are used to calculate the stator and rotor currents and the stator and rotor fluxes. From the latter it is possible to derive the equation of torque and can be written as:

$$T_{em} = \frac{3}{2} \cdot pp \cdot (\lambda_{s\alpha} \cdot i_{s\beta} - \lambda_{s\beta} \cdot i_{s\alpha}) \quad (3.1)$$

The rotor speed is calculated in the mechanic block and it is used in the Induction Motor block to evaluate the components. The Simulink model is as follows:

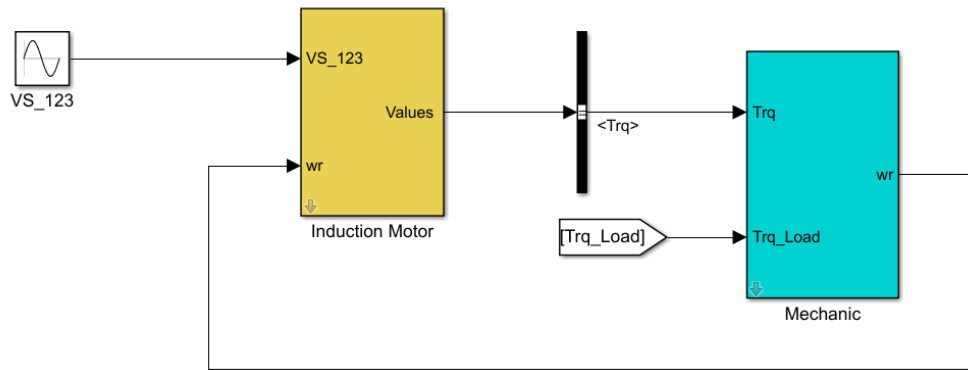


Figure 3.2: Simulink ($\alpha\beta$) model.

Focusing on the Induction Motor block. It was built using the equations in the previous chapter:

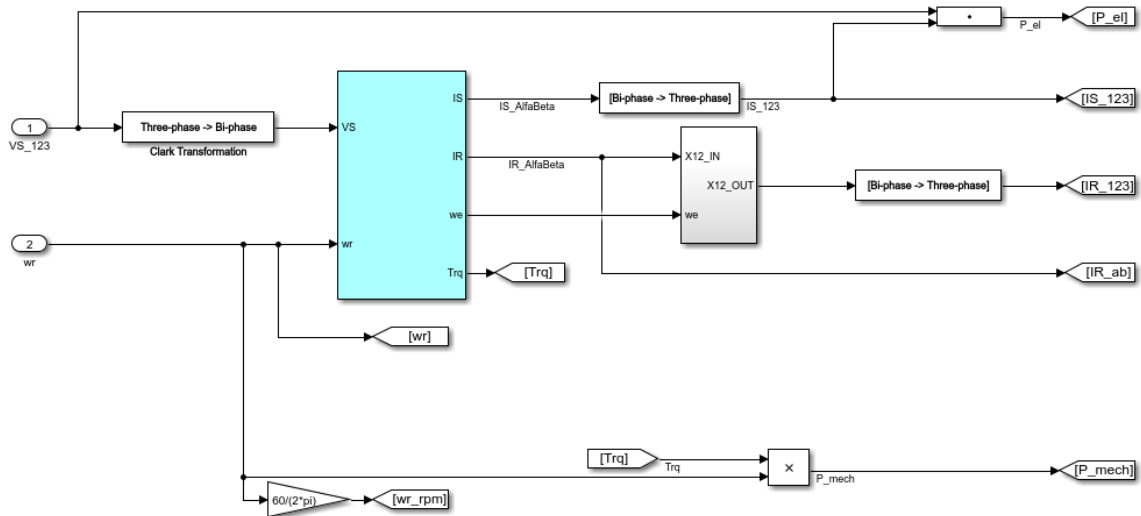


Figure 3.3: Induction Motor Simulink ($\alpha\beta$) model.

The mechanic block has in input the motor torque and the load torque and it gives in output the rotor speed. It is described by this equation:

$$\frac{d\omega_r}{dt} = \frac{Trq - Trq_{load} - K_w \cdot \omega_r}{J_{eq}} \quad (3.2)$$

where J_{eq} is the motor inertia and K_w is the damping coefficient and is equal to zero. The mechanic block can be represent as follows:

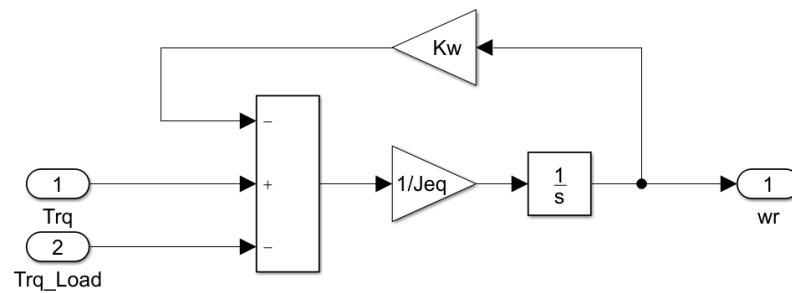


Figure 3.4: Mechanic Simulink model.

3.2 dSPACE general description

dSPACE system uses the Simulink environment and it programs an FPGA instead of a processor. This makes the control environment very fast and it is used for real-time simulations.

The requirements to do this are:

- Xilinx System Generator;
- dSPACE RTI FPGA programming blockset;
- dSPACE free programmable FPGA Board.

Xilinx System Generator is used for the DSP and it uses Simulink to do the FPGA design.

In this thesis work, the Hardware SCALEXIO DS6602 is used.

Models with FPGA applications consist of:

- processor interface;
- FPGA interface.

The processor interface is implemented in Simulink. Also the FPGA interface is implemented in Simulink but it uses the XILINX XSG library.

One of the major problems of the Hardware implementation is that the FPGA is programmed with VHDL code. The Simulink model is not compatible with this code and the model must be changed using compatible blocks. The Simulink blocks are substituted with new blocks

that support the code generated.

The XILINX Blockset convert the Simulink double precision floating-point input to fixed-point. Thanks to the XILINX XSG library all this will be handled automatically.

The real-time target hardware platform used for implementing this thesis work is the SCALEXIO LabBox, presented in Figure 3.8.

dSPACE model is composed of two subsystems. One is related to the processor and the other one is related to the FPGA. In this case, the two systems are not separated but the FPGA one is inside the processor one (*Single – Model Approach*). The reason is that only with this choice you can run the off-line simulation. Otherwise, the two models have to run individually and it is possible only with online simulation (*Double – Model Approach*).

In Figures 3.5 and 3.6 can be possible to see the representation of the Single model approach and Double model approach:

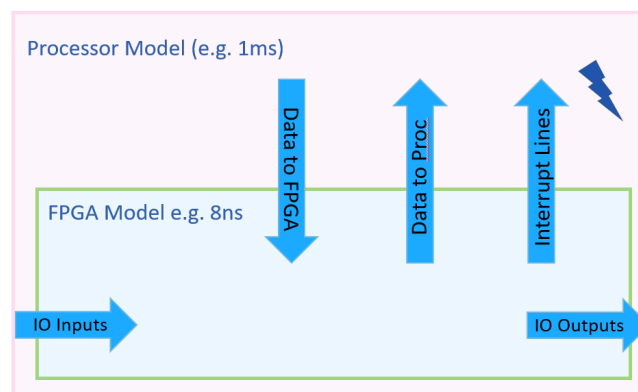


Figure 3.5: Single-Model Approach [7].

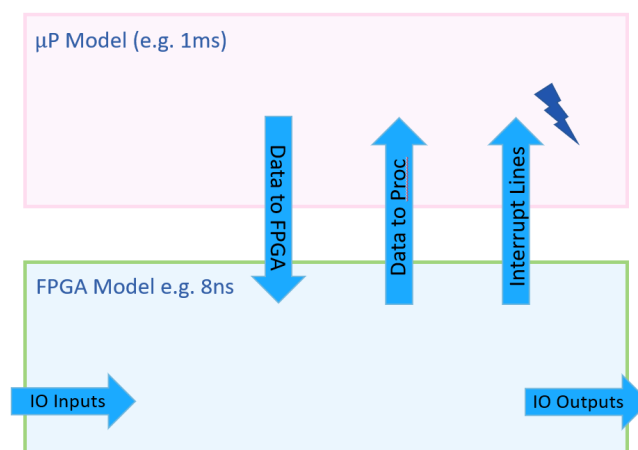


Figure 3.6: Double-Model Approach [7].

The FPGA is a net of semiconductor devices that communicate with each other through a parallel communication. Thanks to this, it works faster and can be used for real-time simulation and thus for Hardware in the Loop (HIL) simulations. On the other hand, Simulink can not be used for real-time (HIL) simulation due to its computational time.

To run the dSPACE simulations, it is used the FPGA Base board DS6602.

The DS6602 is the new High-End FPGA Board and is used for eDrive and power electronics simulations. It provides a Xilinx Kintex-7 FPGA and this can be programmed by users using the RTI FPGA Programming Blockset. The I/O module can be connected to the DS6602.

The technical details are shown in the Figure below:

Technical Details	DS6602
General	User-programmable FPGA board
FPGA	Xilinx® Kintex® UltraScale+™ KU15P <ul style="list-style-type: none"> ▪ System logic cells: 1,143,000 (DSP slices: 1968) ▪ Distributed RAM: 9,800 kbit ▪ Block RAM: 34,600 kbit ▪ Ultra RAM: 36,000 kbit
Additional onboard RAM	4 GB
Angular Processing Units (APUs)	Up to 6 as master or slave
Number of connectors for I/O modules	<ul style="list-style-type: none"> ▪ 5 connectors for standard I/O modules ▪ 1 connector with 4 multi-gigabit transceivers (MGTs)
Device timing	125 MHz
Internal communication interface	IOCNET
Physical size	<ul style="list-style-type: none"> ▪ 238 x 100 x 39 mm (9.4 x 3.9 x 1.5 in) ▪ Requires 2 slots plus one additional slot for each I/O module
Voltage supply	24 V
Typical power consumption	75 W

Figure 3.7: DS6602 FPGA Base Board [8].

The real-time hardware is SCALEXIO LabBox and thanks to the new design is really compact size.



Figure 3.8: SCALEXIO LabBox [7].

SCALEXIO LabBox is used for test drives, in the development of components such as electric powertrains. To produce the HIL procedure, after having collected the inputs and the outputs of the simulation, the Simulink model is transformed and all the blocks that are not included in the code generation phase will be removed. The generated VHDL code is inserted in SCALEXIO LabBox to perform real-time simulations.

The blocks and the equations used will be analysed to see if the models work in the same or in different ways.

3.3 Overview on dSPACE model

The dSPACE model can be modelled as Figure 3.1. Like for the Simulink model also in this case the equations used are written in the Chapter 1.

In the dSPACE model there are two interfaces:

- **Processor interface:** in this interface can be possible to use the Simulink blocks and the input values of the motor are provided.
- **FPGA interface:** the machine equations are solved.

In the figures below, the processor and the FPGA interfaces can be see:

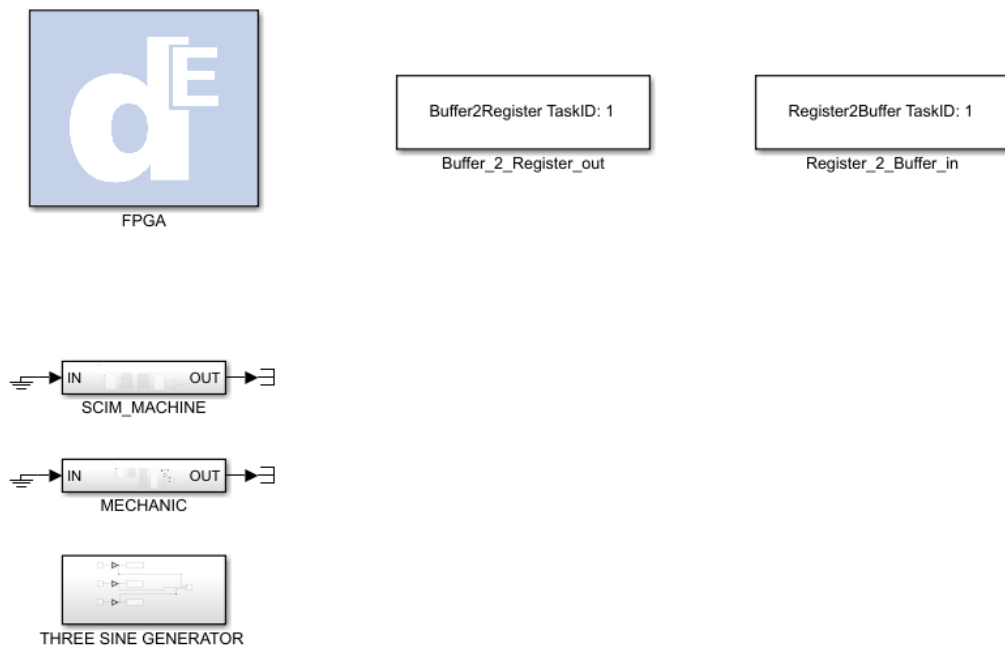


Figure 3.9: dSPACE processor interface.

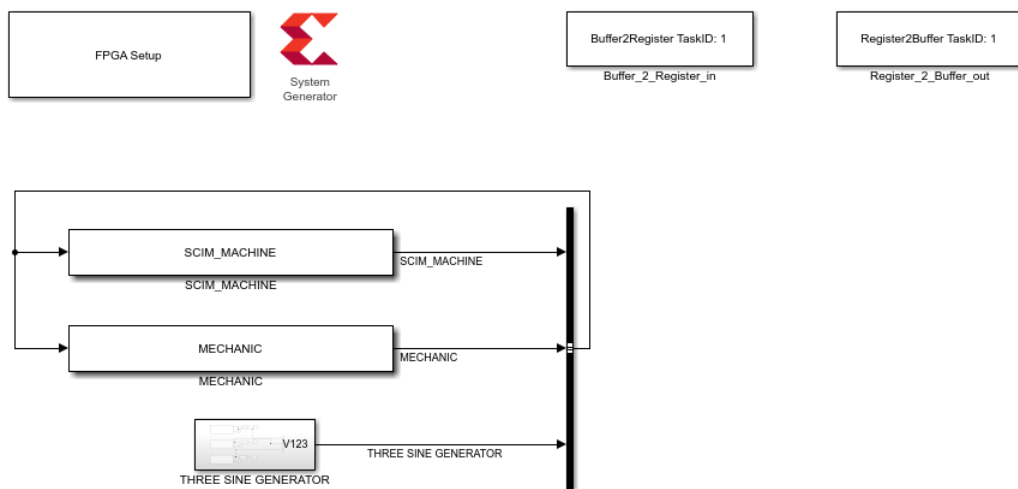


Figure 3.10: dSPACE FPGA interface.

In dSPACE XSG model the processor communicates with the FPGA through the *Buffer2Register* and the *Register2Buffer* blocks.

- **Buffer2Register:** the buffer is a vector of data from the RTIFPGA library. It has the task to reads out the buffer on the FPGA side. This information is sent from the processor side. This information is sent from the processor side. It stores this

information into register blocks and they are transported in the FPGA model and it contains the parameterization of the FPGA components. It provides the functionality serial to parallel.

- **Register2Buffer:** it merges several register signals to a buffer which information are received on the processor side. It contains the feedback signals from the FPGA components. It provides the functionality parallel to serial.

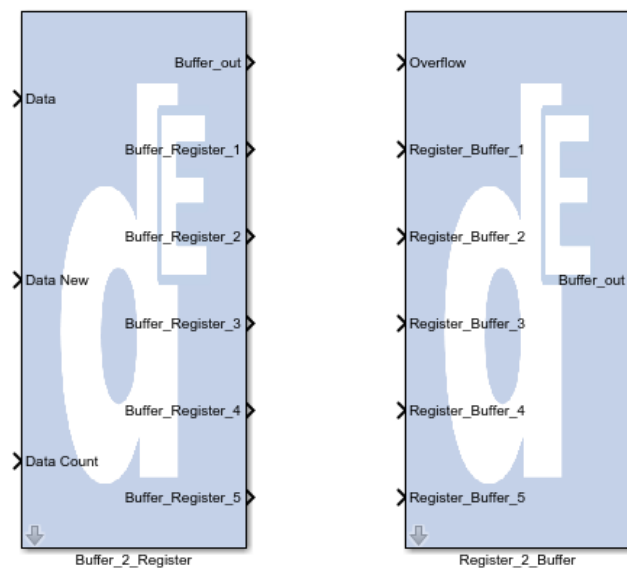


Figure 3.11: Buffer2Register and Register2Buffer blocks [9].

If the off-line simulation is set within the Buffer2Register and Register2Buffer blocks, the communication via processor and FPGA and vice versa is done directly bypassing the RTIFPGA library, as shown below:

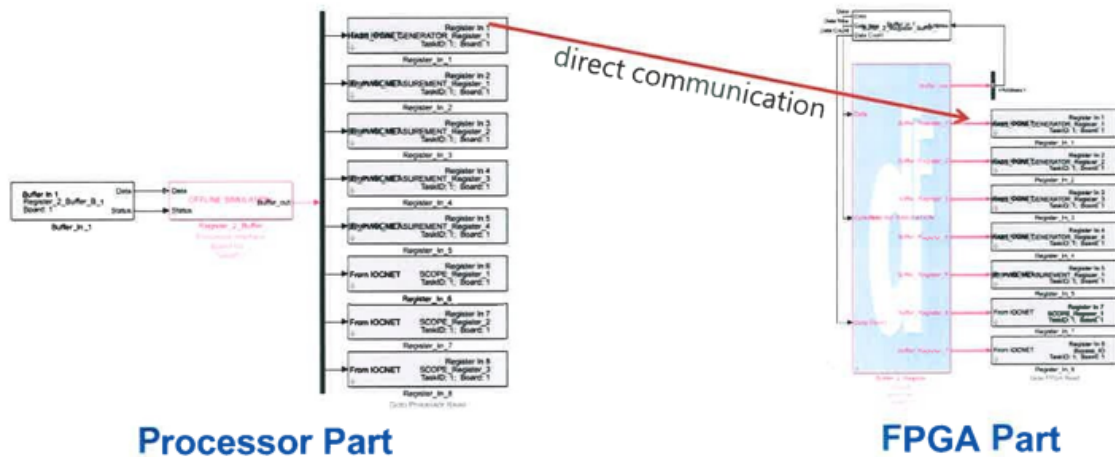


Figure 3.12: Processor part and FPGA part direct communication [9].

In the dSPACE model is possible to choose if used the Amplitude or Power invariant Clark transformation. The goal of the activity is to compare the models, so also in this case the *Amplitude invariant* matrix is used.

In this case, the Induction Motor model is more complex with respect to the Simulink model, because it has many conversions, indeed it works with bits that are assigned to the registers of the variables.

The Figure 3.14 shows the FPGA interface SCIM Machine model.

In this block, the electric and magnetic equations are developed and motor torque, stator and rotor currents, mechanical and electrical powers are calculated.

The mechanical block, also in this case, is represented by 3.2. Therefore, the rotor speed ω_r is calculated and this is used to computes the actual position of the rotating system through the Angular Processing Unit (APU). The APU block is included in the mechanical one. The APU interface bus is connected to the other components of the same rotating system, as in this case, the SCIM machine. The rotor speed ω_r , as in the previous case, is used in the SCIM machine to calculate the motor torque.

The Figure 3.14 shows the FPGA interface Mechanic model.

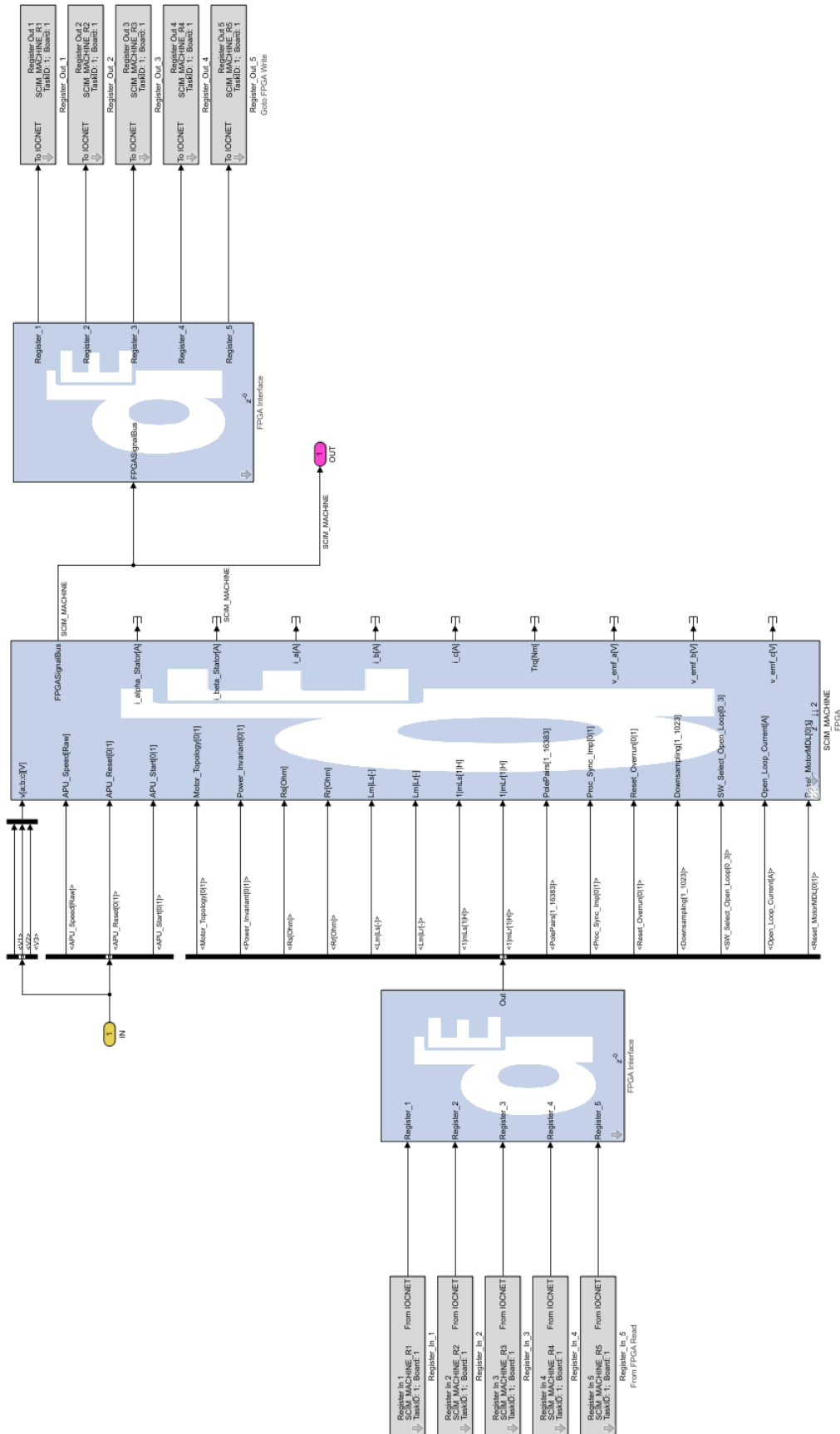


Figure 3.13: SCIM Machine block FPGA interface.

3.4 Simulink and dSPACE results comparison

Simulink and dSPACE models have been compared in this section. To compare the software, the parameters used are those of the dynamic course of electrical machines carried out at the Politecnico di Torino.

In this thesis, iron losses and magnetic saturation were not treated.

The implementation of the model is used to study the dynamic behaviour of the IM. The characteristics of the motor are given in the table below:

Table 3.1: Characteristics of the motor.

<i>Number</i>	<i>MA112M4</i>	<i>Reference temperature, T_{ref}</i>	75°
P_{nom}	<i>4kW</i>	<i>Magnetizing reactance, X_m</i>	44.2Ω
$V_{nom,phase}$	<i>220V</i>	<i>Iron resistance, R_{fe}</i>	1146Ω
$I_{nom,phase}$	<i>9.0A</i>	<i>Stator Resistance, R_s</i>	1.000Ω
f_{nom}	<i>50Hz</i>	<i>Rotor Resistance, R_r</i>	1.145Ω
n_{nom}	<i>1400rpm</i>	<i>Stator reactance, $X_{\sigma S}$</i>	1.575Ω
<i>Service</i>	<i>S1</i>	<i>Rotor reactance, $X_{\sigma R}$</i>	1.612Ω

The values are calculated with no-load and locked-rotor tests and they are the same under dynamic and in steady-state conditions.

The main parameters of the motor are shown in the table:

Table 3.2: Parameters of the Induction Motor.

Parameters of the Induction Motor	Value
<i>Stator Resistance (Ω)</i>	1
<i>Rotor Resistance (Ω)</i>	1.145
<i>Stator Inductance (H)</i>	0.1457
<i>Rotor Inductance (H)</i>	0.1458
<i>Mutual Inductance (H)</i>	0.1406
<i>Pole Pairs</i>	2

Table 3.3: Parameters of the Mechanic block.

Parameters of the Mechanic block	Value
<i>Load Inertia (kgm²)</i>	0.12
<i>Motor Inertia (kgm²)</i>	0.05
<i>Total Inertia (kgm²)</i>	0.17
<i>Torque Load (Nm)</i>	26.5

The time-step of the simulations was imposed to 10^{-6} seconds.

The simulations were performed with a three-phase voltage source at 200V and 50Hz, at 220V and 60Hz, at 380V and 40Hz and 380V and 60Hz.

3.4.1 Simulation: 220V - 50Hz

In the following section are reported the results of the simulation with 220V and 50Hz.

The simulations are performed in the same way in Simulink and dSPACE. dSPACE is currently being used to run the simulation in off-line mode.

The dSPACE model in off-line simulations simulates the behaviour of the FPGA. The FPGA and the processor model part are in the same model but in different subsystem. This entails the fact that is not necessary to make the build of the model but in this case, the simulations are very slow.

From the comparisons between Simulink and dSPACE is possible to see the following quantities:

- Stator Currents;
- Motor Torque;
- Electrical Power;
- Mechanical Power;
- Rotor Speed;
- Stator Flux;

- Rotor Flux.

The steady-state simulations results have been reported in the table below:

Table 3.4: Steady-state Simulink simulation - 220V-50Hz.

Simulink Simulation	Value
<i>Rotor Speed (rpm)</i>	1443
<i>Mechanical Power (kW)</i>	4.005
<i>Electrical Power (kVA)</i>	4.375
<i>Stator flux α phase (Wb)</i>	-0.960
<i>Stator flux β phase (Wb)</i>	-0.023
<i>Rotor flux α phase (Wb)</i>	-0.919
<i>Rotor flux β phase (Wb)</i>	0.074

Table 3.5: Steady-state dSPACE simulation - 220V-50Hz.

dSPACE Simulation	Value
<i>Rotor Speed (rpm)</i>	1443
<i>Mechanical Power (kW)</i>	4.003
<i>Electrical Power (kVA)</i>	4.373
<i>Stator flux α phase (Wb)</i>	-0.960
<i>Stator flux β phase (Wb)</i>	-0.022
<i>Rotor flux α phase (Wb)</i>	-0.919
<i>Rotor flux β phase (Wb)</i>	0.075

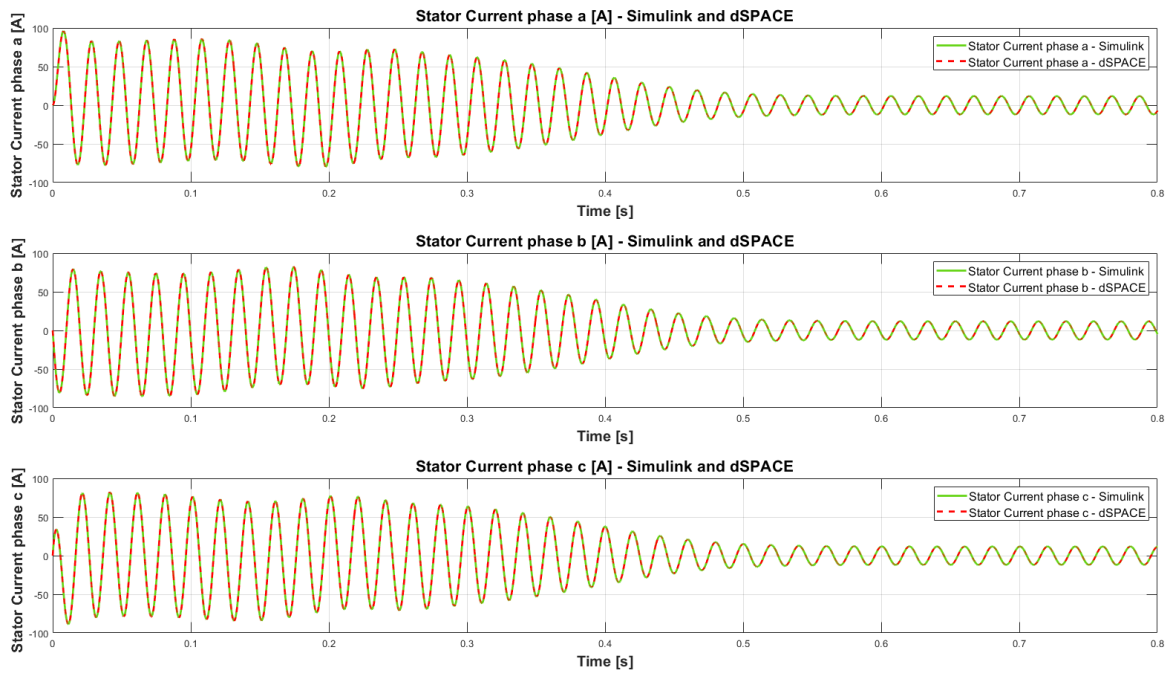


Figure 3.15: Stator Currents i_a - 220V-50Hz.

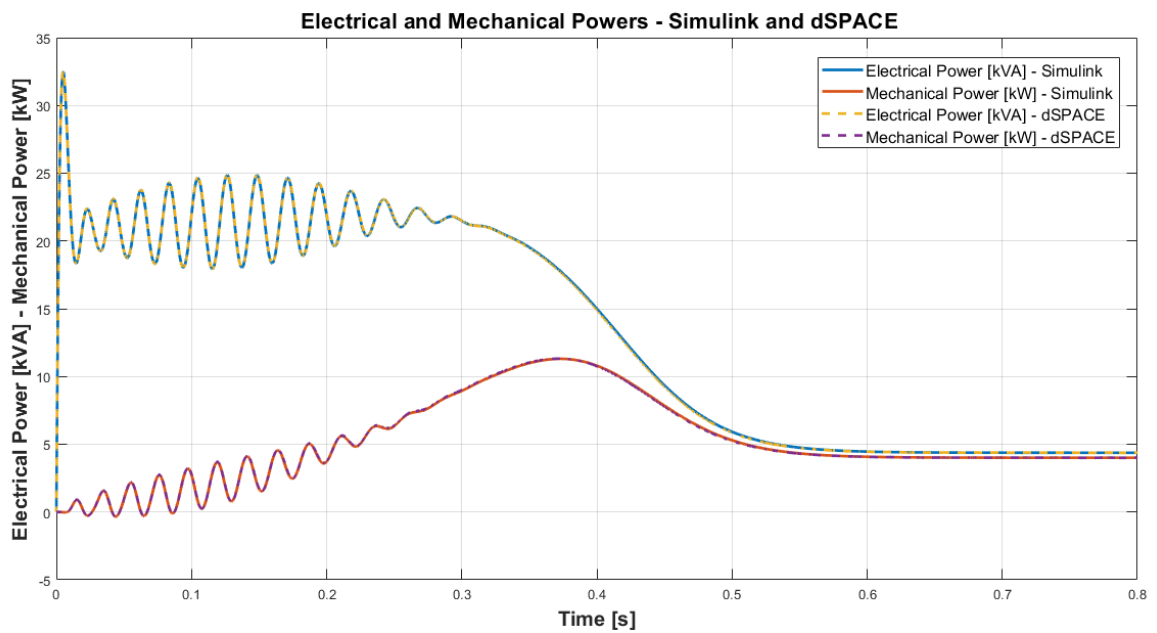


Figure 3.16: Electrical and Mechanical Powers - 220V-50Hz.

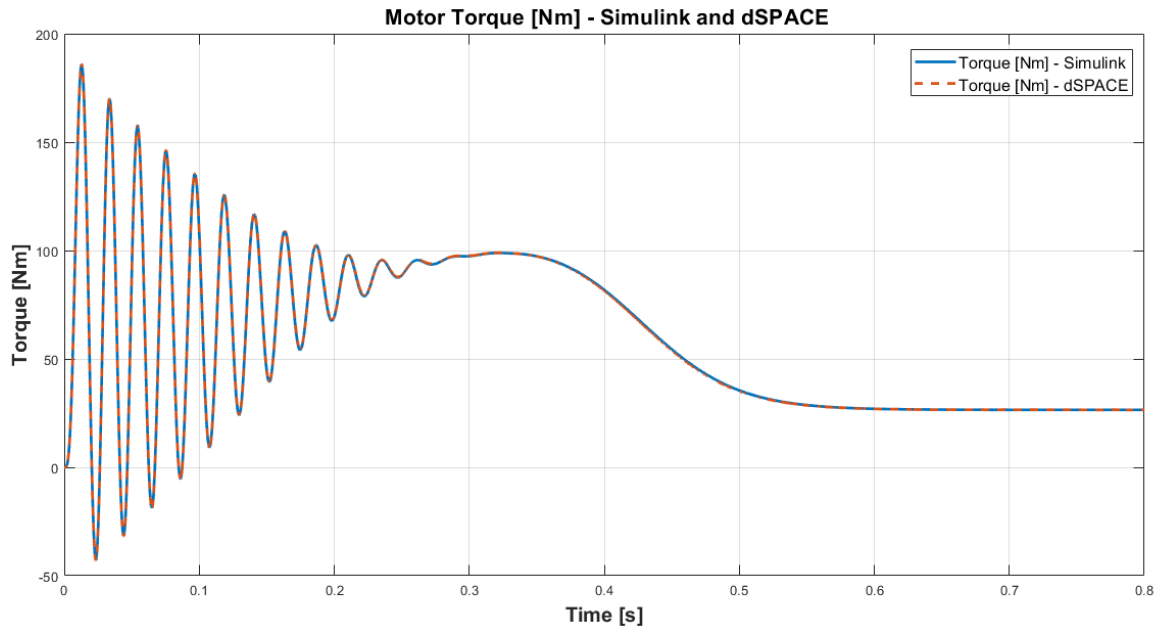


Figure 3.17: Motor Torque - 220V-50Hz - 220V-50Hz.

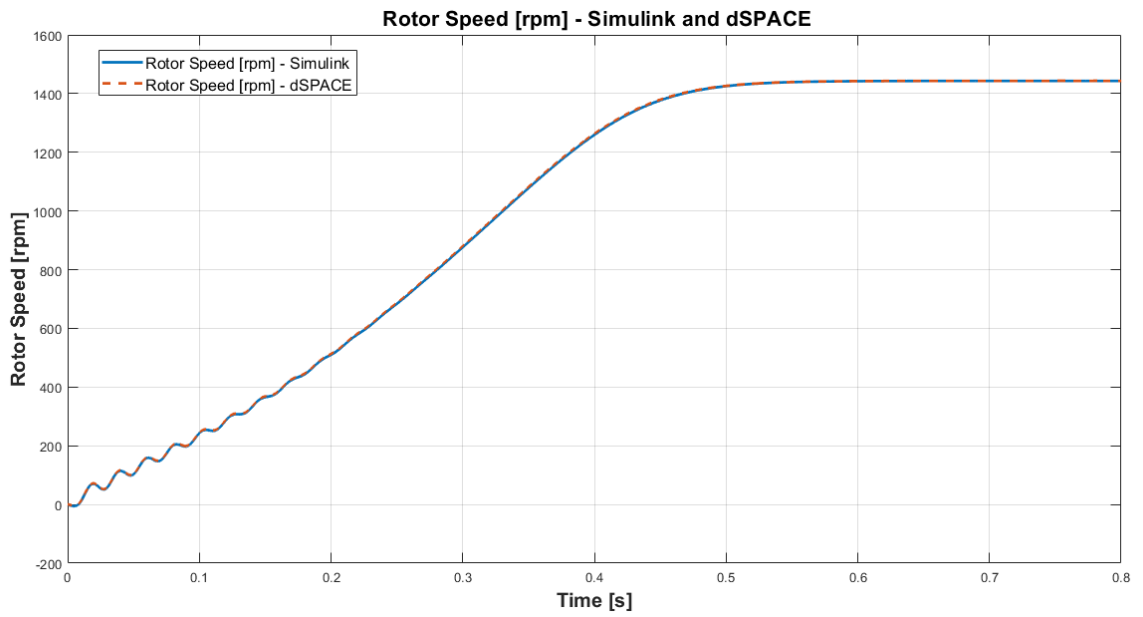


Figure 3.18: Rotor Speed - 220V-50Hz.

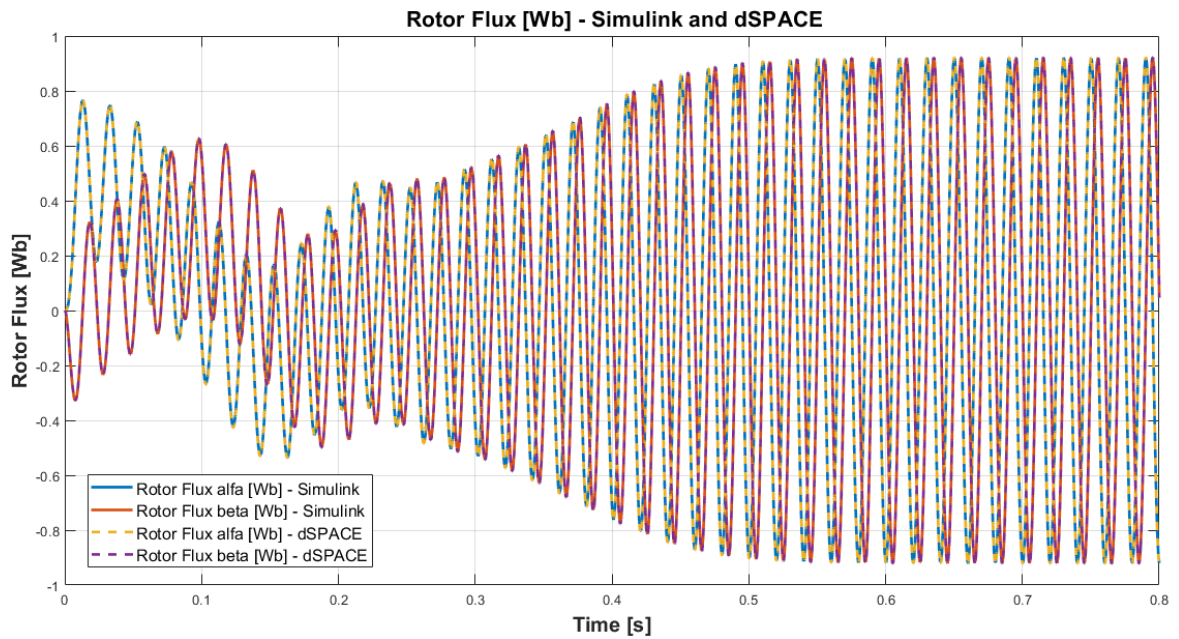


Figure 3.19: Rotor Flux - 220V-50Hz.

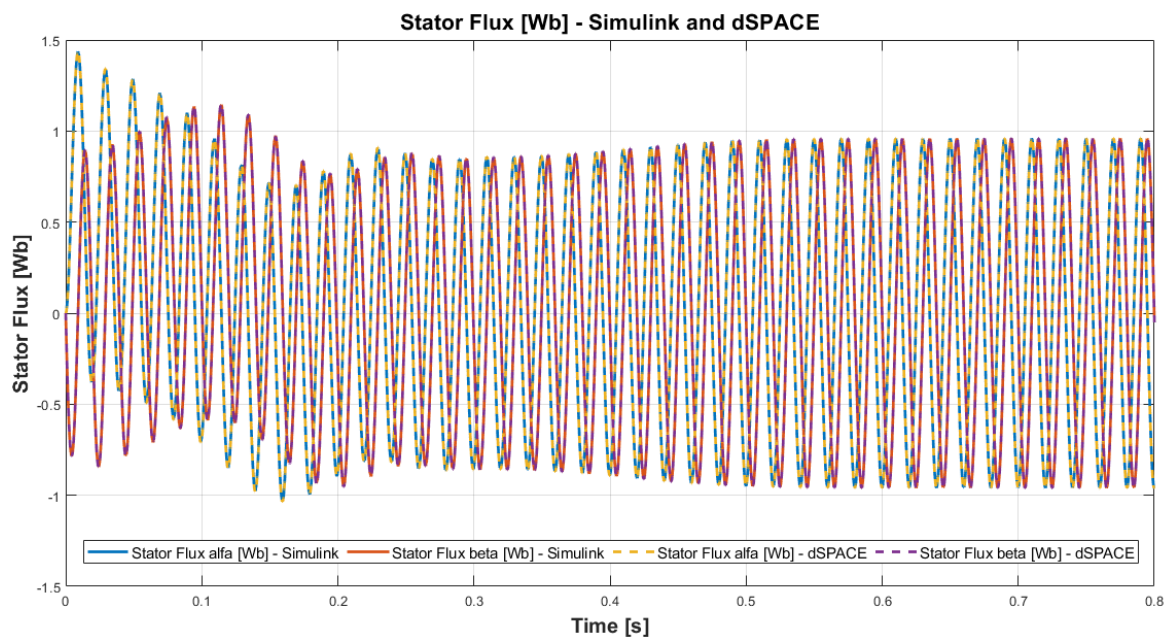


Figure 3.20: Stator Flux - 220V-50Hz.

For the rotor currents in three-phase coordinates it is possible to notice how the frequency of the rotor decreases when the rotor speed increases until they become zero.

The motor torque has oscillations due to the unipolar components of the currents. The unidirectional components generate a fixed continuous field that interacts with the rotating field. The latter is created by the alternative components of the stator and rotor currents.

When the unidirectional components became zero, the motor torque oscillations also become zero. When the load torque is applied the motor slows down. In this way, the stator currents are induced.

3.4.2 Simulation: 380V - 40Hz

In this section are reported the results of the simulations with 380V and 40Hz. These simulations were made to be sure that the software also with different frequencies and voltages respond in the same way. The quantities analysed are the same as in the previous section.

From the simulation the following steady-state results have been obtained:

Table 3.6: Steady-state Simulink simulation - 380V-40Hz.

Simulink Simulation	Value
<i>Rotor Speed (rpm)</i>	1188
<i>Mechanical Power (kW)</i>	3.298
<i>Electrical Power (kVA)</i>	3.678
<i>Stator flux α phase (Wb)</i>	-2.120
<i>Stator flux β phase (Wb)</i>	-0.057
<i>Rotor flux α phase (Wb)</i>	-2.096
<i>Rotor flux β phase (Wb)</i>	-0.012

Table 3.7: Steady-state dSPACE simulation - 380V-40Hz.

dSPACE Simulation	Value
<i>Rotor Speed (rpm)</i>	1187
<i>Mechanical Power (kW)</i>	3.299
<i>Electrical Power (kVA)</i>	3.678
<i>Stator flux α phase (Wb)</i>	-2.120
<i>Stator flux β phase (Wb)</i>	-0.055
<i>Rotor flux α phase (Wb)</i>	-2.047
<i>Rotor flux β phase (Wb)</i>	-0.010

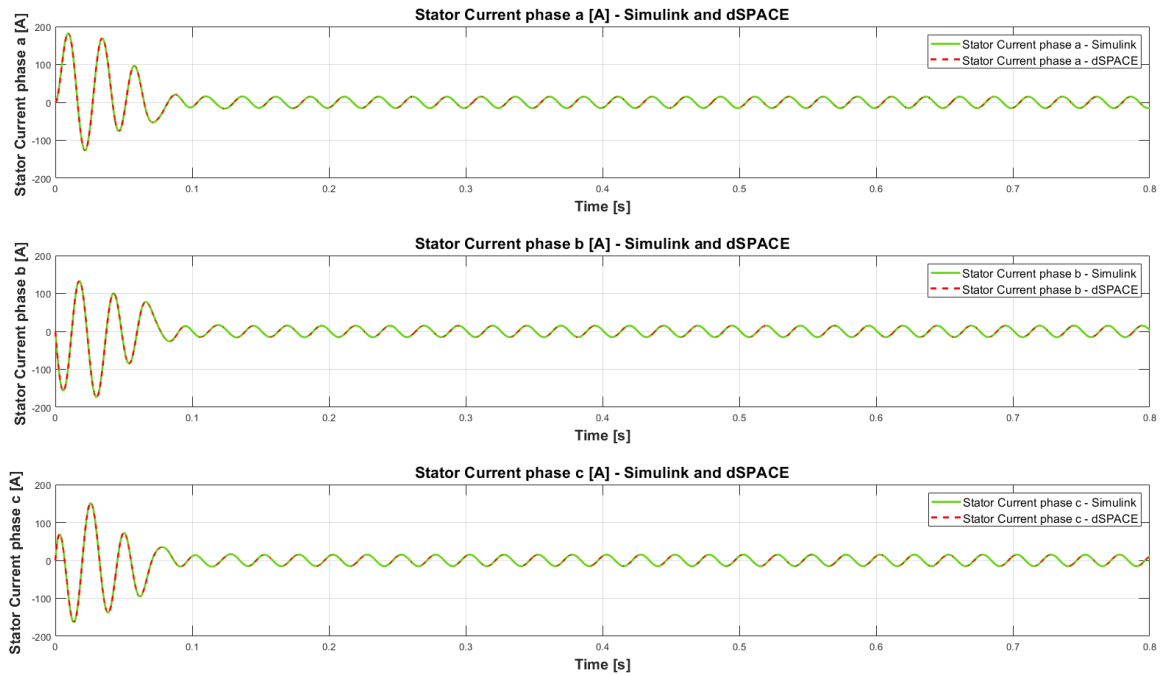


Figure 3.21: Stator Currents i_a - 380V-40Hz.

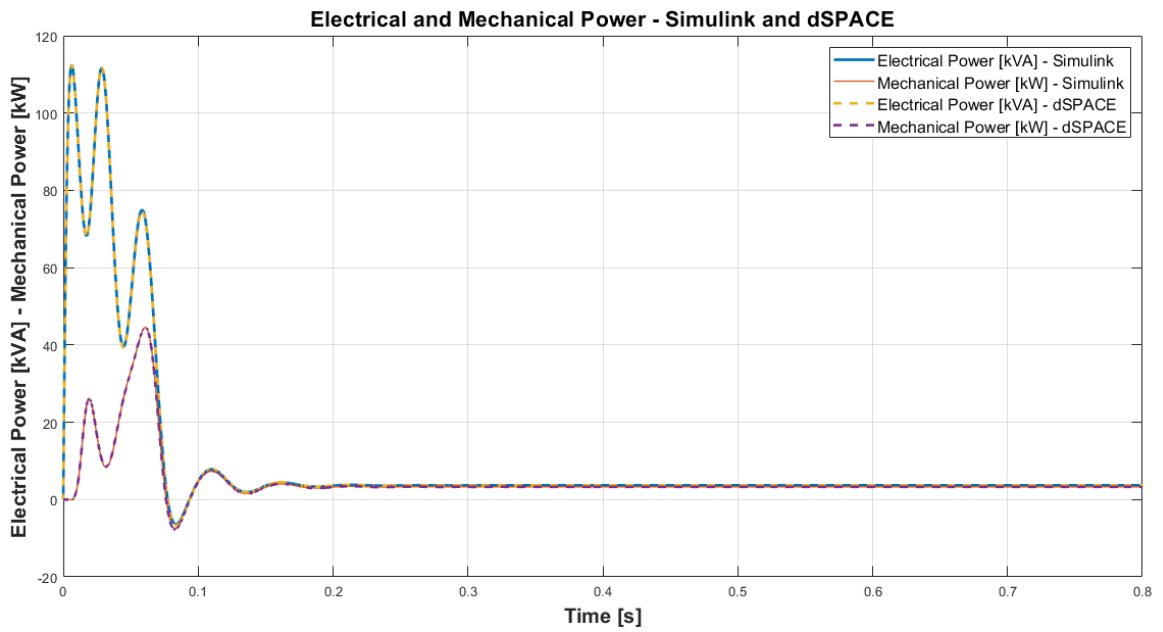


Figure 3.22: Electrical and Mechanical Powers - 380V-40Hz.

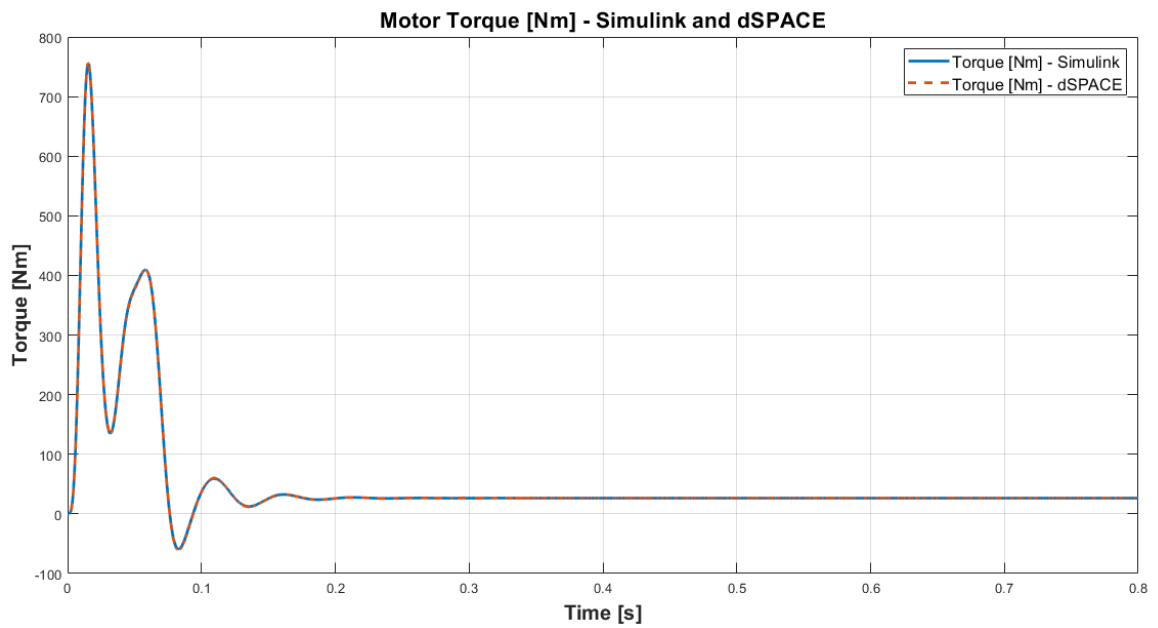


Figure 3.23: Motor Torque - 380V-40Hz.

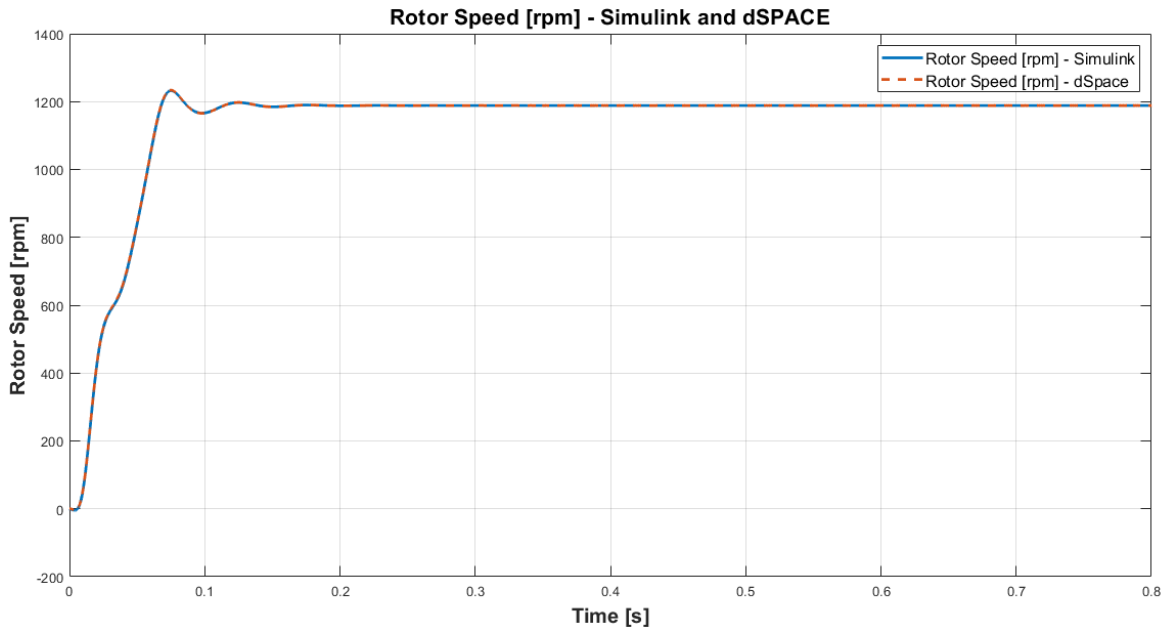


Figure 3.24: Rotor Speed - 380V-40Hz.

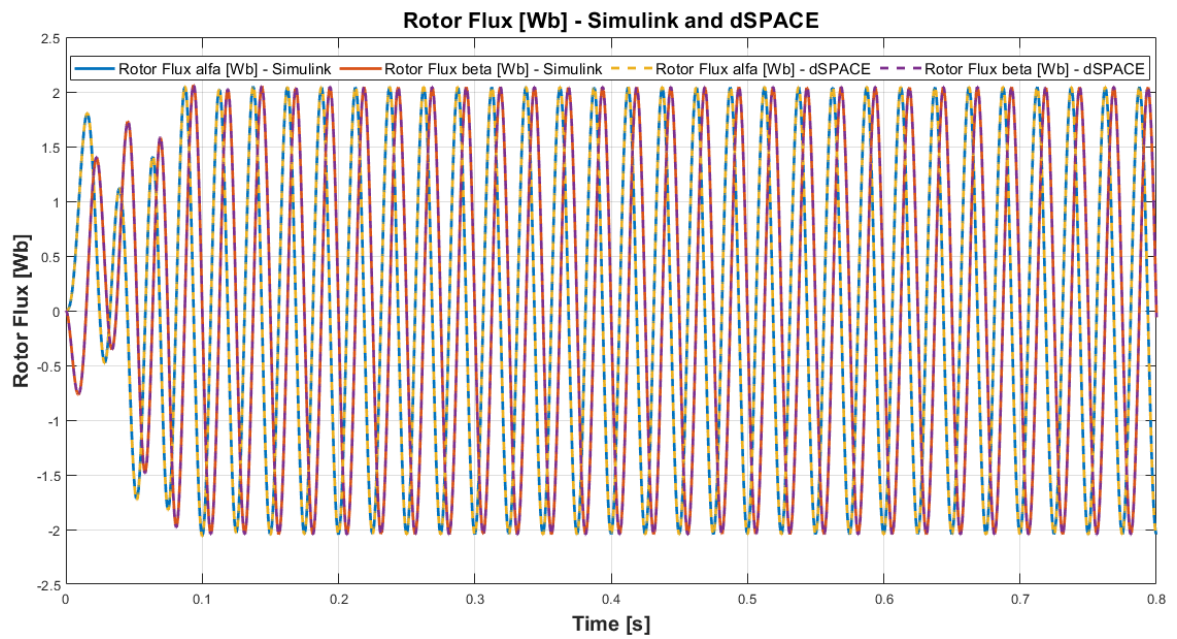


Figure 3.25: Rotor Flux - 380V-40Hz.

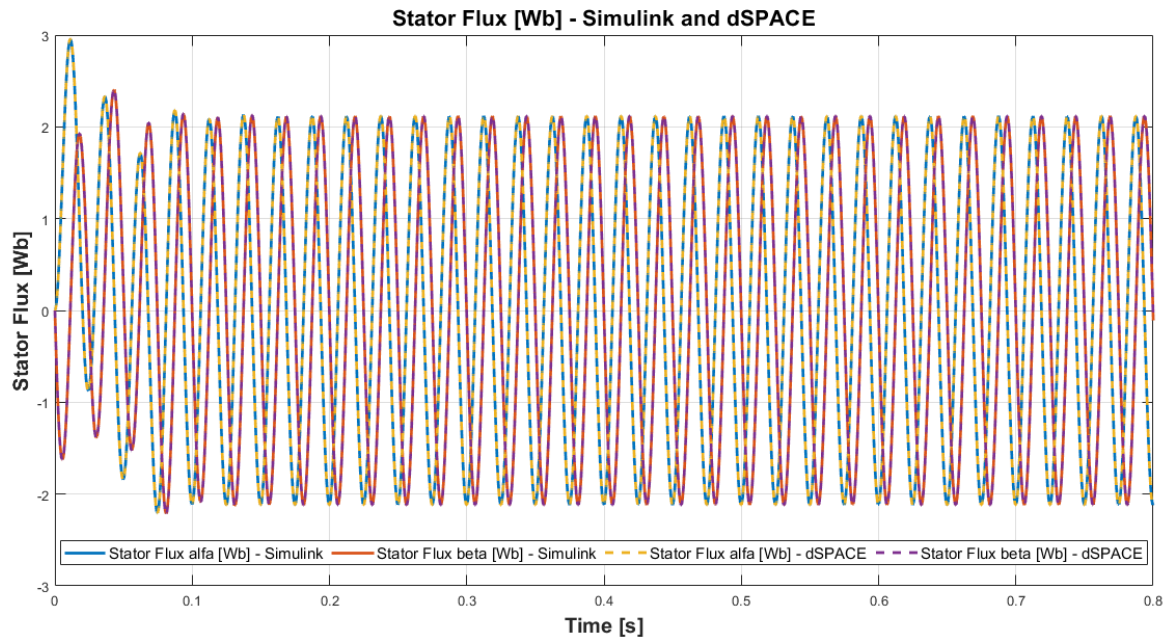


Figure 3.26: Stator Flux - 380V-40Hz.

The figures in the previous images showed that Matlab/Simulink and dSPACE give the same results in off-line simulations. As the theory shows, when the frequency is lower the rotor speed also decreases.

Chapter 4

Real-time simulations

The difference between real-time simulations and off-line simulations is the time of these. In the electrical environment, real-time simulations are not a new idea. Hardware in the loop (HIL) simulations of these systems require an innovative approach.

The real-time simulations can be divided into three groups: [10]

- fully digital simulation;
- controller HIL (CHIL) simulation;
- power HIL (PHIL) simulation.

The topics of this chapter are the real-time simulations of the model described in Chapter 3.

These simulations are made using the $(\alpha\beta)$ and the (dq) reference frame.

As it is possible to see in the previous sections, off-line comparisons are made only in $(\alpha\beta)$ reference frames.

This is because in dSPACE the (dq) reference frames use only time-step $8 \cdot 10^{-9}$ seconds and, in this case, the simulations are very slow.

Therefore, the idea is to create the (dq) model just for a real-time environment.

4.1 FPGA build process

To prepare the model for real-time simulations it is necessary to build the model. To do this, the simulations time-step must be set $8 \cdot 10^{-9}$ seconds and the FPGA Setup and System Generator blocks are essential.

In the Figure below an example of these blocks:



Figure 4.1: FPGA Setup and System Generator.

In the FPGA Setup subsystem is possible to confirm the selection and validate the execution of the build.

FPGA buit result is an ini. file and it is import in the tool ConfigurationDesk.

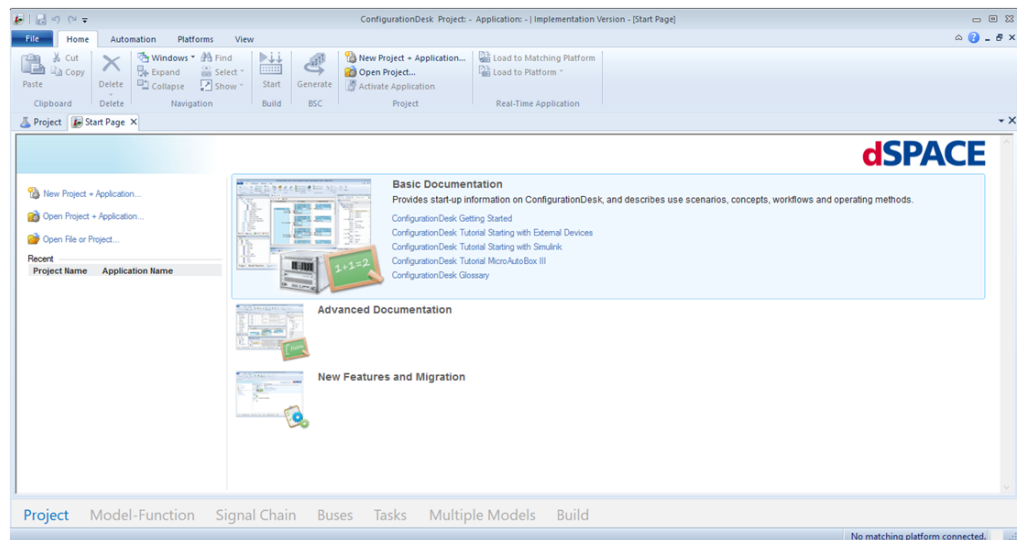


Figure 4.2: ConfigurationDesk interface.

With ConfigurationDesk the Simulink model can be deployed and to do this it is necessary to configure the SCALEXIO hardware.

This tool generates real-time applications that will be run in a real-time system.

After the project is built, the ControDesk 7.2 tool is used to download and launch applications in real-time.

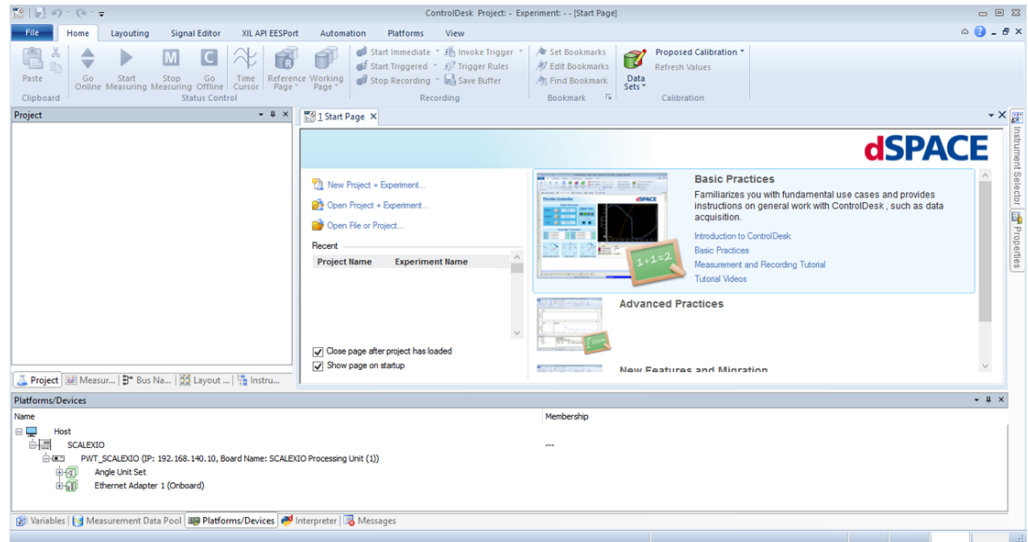


Figure 4.3: ControlDesk interface.

Thanks to this software, it is possible to see and change the parameters online.

4.2 Comparison between Simulink and dSPACE real-time simulations ($\alpha\beta$) reference frame

The goal of this activity was to implement Simulink and dSPACE models first in off-line mode and, after making comparisons, compare models in online mode.

Following the implementation of the Induction motor in the ($\alpha\beta$) reference frame, real-time comparisons have been made.

The parameters used are the same as the off-line simulations and they are shown in the Table 5.5.

The simulation performed with a three-phase voltage of 220V and a frequency of 50Hz.

The model is prepared for real-time simulation, then the FPGA block is commented and the input values inserted in the processor interface are send directly to the physical FPGA.

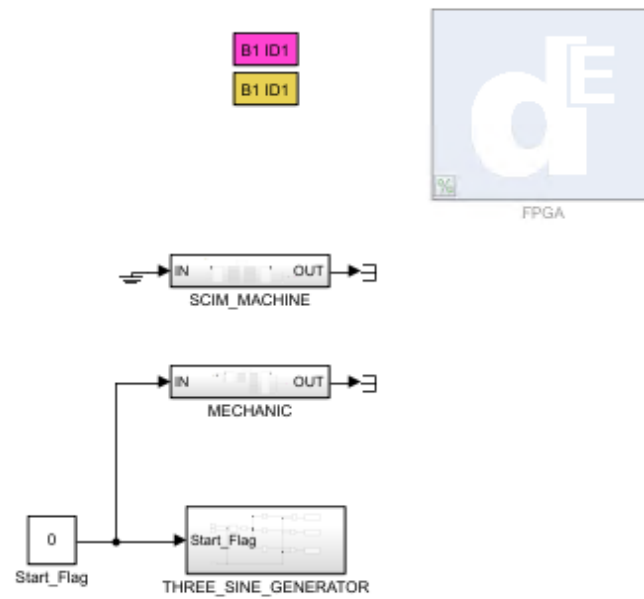


Figure 4.4: FPGA model comment out.

From the comparisons between Simulink and dSPACE is possible to see the following quantities:

- Stator current;
- Rotor speed.

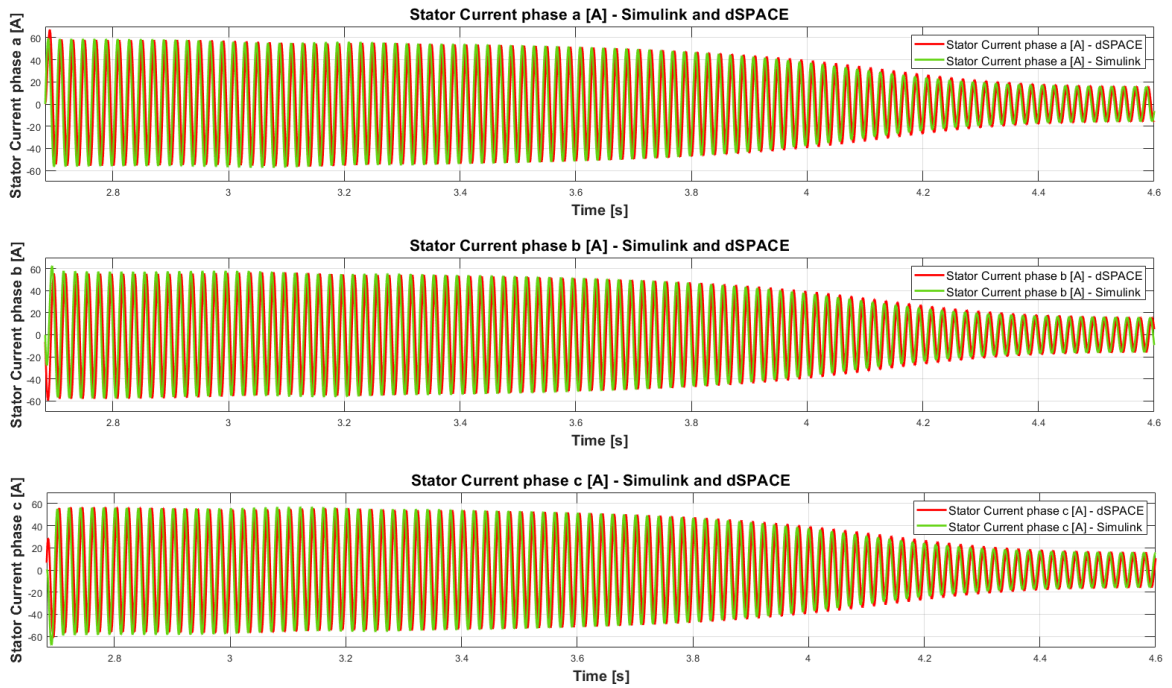


Figure 4.5: Stator current Simulink and dSPACE real-time.

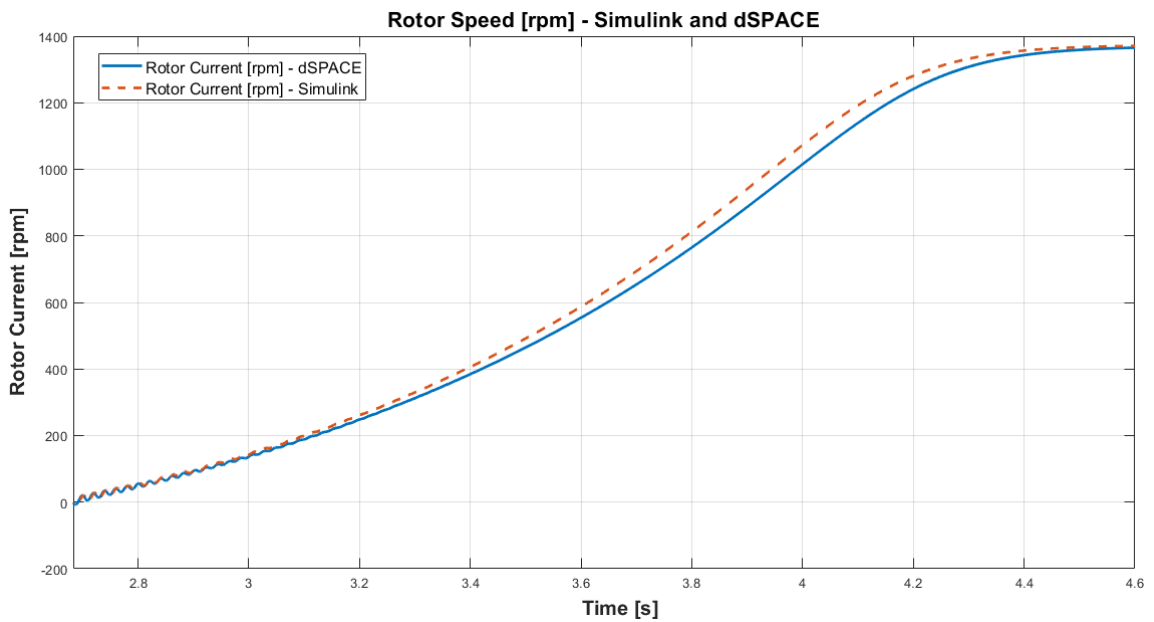


Figure 4.6: Rotor speed Simulink and dSPACE real-time.

About these comparisons, it is possible to say that also the real-time simulations the results are in agreement between the $(\alpha\beta)$ model in Simulink and dSPACE real-time.

4.3 Comparison between Simulink and dSPACE real-time simulations (dq) reference frame

As mentioned in the introduction, one of the thesis goals was to develop the model also in (dq) reference frame, so as to evaluate the response in Matlab/Simulink and in dSPACE. To make an off-line simulation with FPGA of this model has not been possible, since being a little diffused model, it was necessary to change too much the dSPACE model. For this reason, real-time simulations were made directly.

Starting from the equations analysed in Section 2.4, the Simulink (dq) model has been realised. It was implemented starting from the Simulink ($\alpha\beta$) model and applying the rotational matrix shown in (2.30). Through the equations mentioned in Chapter 1, quantities of the (dq) model are calculated.

The (dq) model is used in control applications and is different from the ($\alpha\beta$) model because it converts the amount of sinusoidal voltage quantities into (dq) quantities.

In the figures below the Simulink (dq) model is shows:

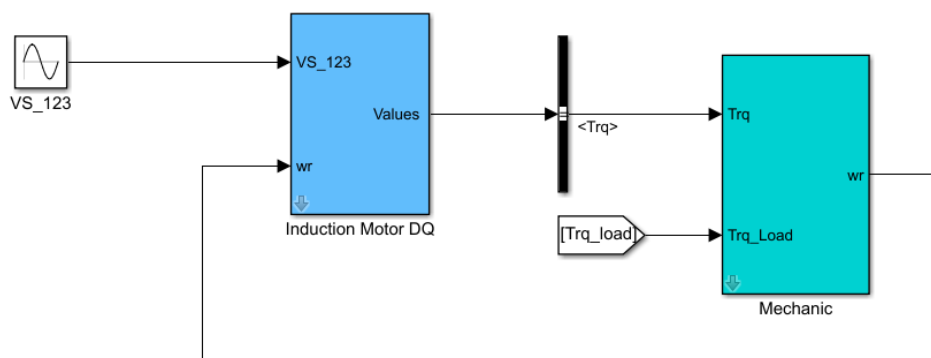
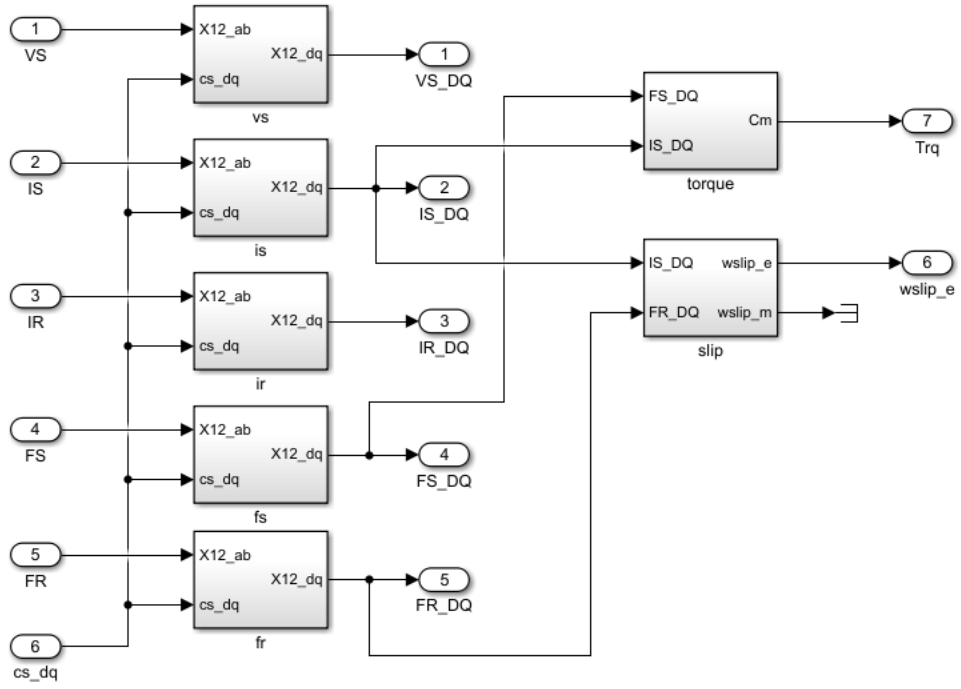


Figure 4.7: Simulink (dq) model.

In the Induction Motor (dq) block the equations were developed and the model was created.

In the grey blocks below, the rotational matrix, shown in (2.30), is executed and the quantities are transformed from ($\alpha\beta$) coordinates to (dq) quantity.


 Figure 4.8: Induction Motor Simulink (dq) model.

The mechanic block is described by the (3.2), as in the ($\alpha\beta$) model. Again, the motor torque generated within the Induction motor (dq) model is an input of the mechanic block. The load torque is set as in the Table 3.3.

After developing the Simulink (dq) model, the dSPACE (dq) model has been studied. The latter has been developed starting from the following equations [11]:

$$\begin{cases} \mathbf{u}_s^f = R_s \cdot \mathbf{i}_s^f + \frac{d\phi_s^f}{dt} + j \cdot \omega_s \cdot \phi_s^f \\ 0 = R_r \cdot \mathbf{i}_r^f + \frac{d\phi_r^f}{dt} + j \cdot \omega_r \cdot \phi_r^f \\ \phi_s^f = L_s \cdot \mathbf{i}_s^f + L_m \cdot \mathbf{i}_r^f \\ \phi_r^f = L_m \cdot \mathbf{i}_s^f + L_r \cdot \mathbf{i}_r^f \end{cases} \quad (4.1)$$

where u_s^f is the stator voltage, R_s and R_r are the stator and the rotor resistances, i_s and i_r are the stator and the rotor currents, ω_s and ω_e are the angular velocity of the stator sides and rotor side, ϕ_s^f and ϕ_r^f are the stator and rotor flux vectors.

L_m is the mutual inductance, L_s is the stator inductance and L_r is the rotor inductance.

As in the stationary reference frame ($\alpha\beta$) the not measurable rotor current as well as the stator flux are eliminated.

Applying mathematical substitutions within the Equation 4.1, the following system is obtained:

$$\begin{cases} \frac{di_{sd}}{dt} = -\left(\frac{1}{\sigma \cdot T_s} + \frac{1-\sigma}{\sigma \cdot T_r}\right) \cdot i_{sd} + \omega_s \cdot i_{sq} + \frac{1-\sigma}{\sigma \cdot T_r} \cdot \phi'_{rd} + \frac{1-\sigma}{\sigma} \cdot \omega \cdot \phi'_{rq} + \frac{1}{\sigma \cdot L_s} \cdot u_{sd} \\ \frac{di_{sq}}{dt} = -\omega_s \cdot i_{sd} - \left(\frac{1}{\sigma \cdot T_s} + \frac{1-\sigma}{\sigma \cdot T_r}\right) \cdot i_{sq} - \frac{1-\sigma}{\sigma} \cdot \omega \cdot \phi'_{rd} + \frac{1-\sigma}{\sigma \cdot T_r} \cdot \phi'_{rq} + \frac{1}{\sigma \cdot L_s} \cdot u_{sq} \\ \frac{d\phi'_{rd}}{dt} = \frac{1}{T_r} \cdot i_{sd} - \frac{1}{T_r} \cdot \phi'_{rd} + (\omega_s - \omega) \cdot \phi'_{rq} \\ \frac{d\phi'_{rq}}{dt} = \frac{1}{T_r} \cdot i_{sq} - (\omega_s - \omega) \cdot \phi'_{rd} - \frac{1}{T_r} \cdot \phi'_{rq} \end{cases} \quad (4.2)$$

where:

- $\phi'_{rd} = \frac{\phi_{rd}}{L_m}$
- $\phi'_{rq} = \frac{\phi_{rq}}{L_m}$
- $\omega_r = \omega_s - \omega$

By fixing the rotor's flux vector to the real axis of the coordinate system, the ϕ_{rq} is set to zero.

Debugging the dSPACE model, some inconsistencies appeared.

The clearest inconsistency is the following:

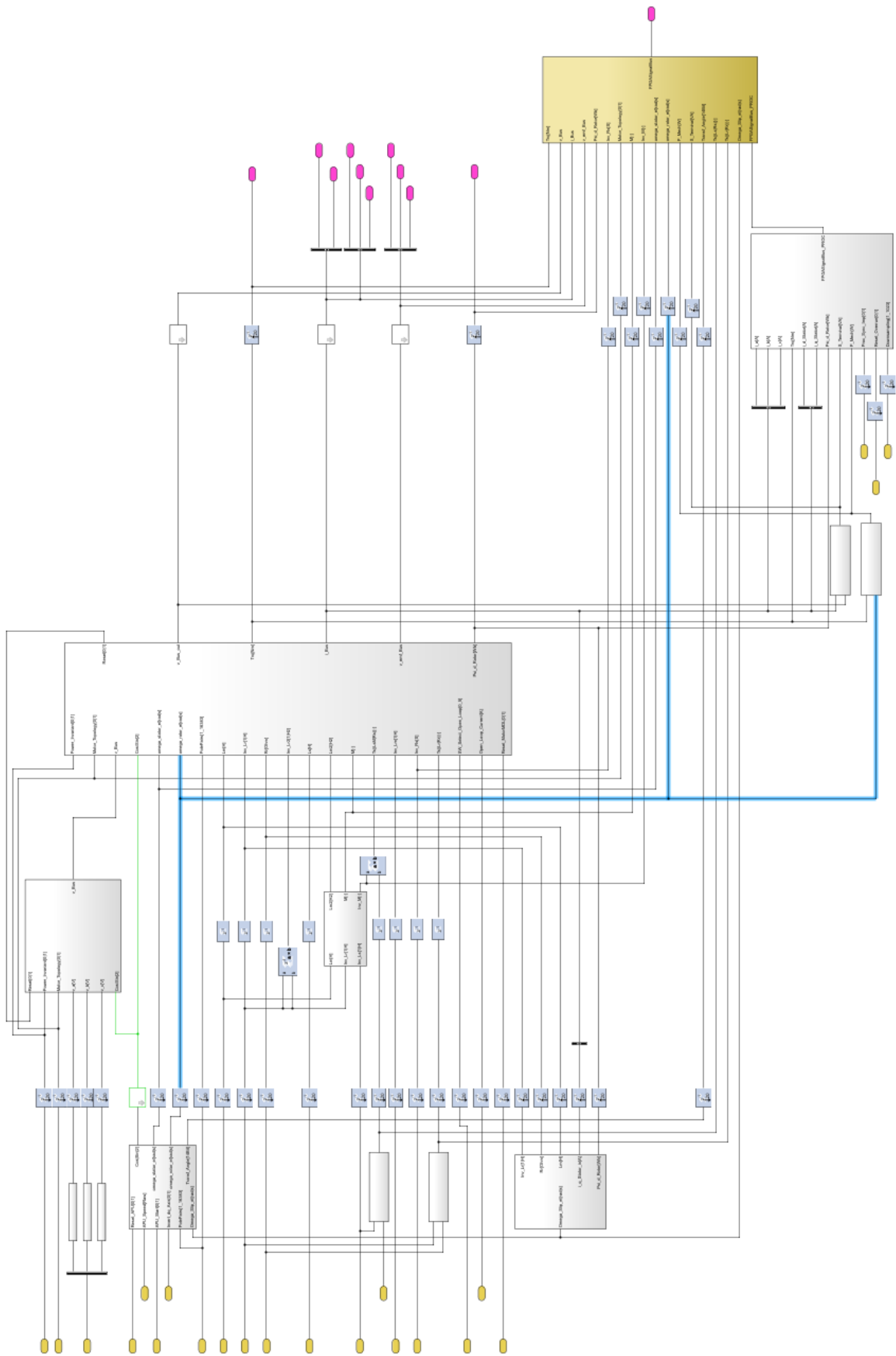


Figure 4.9: Calculate of Mechanical Power dSPACE (dq) model.

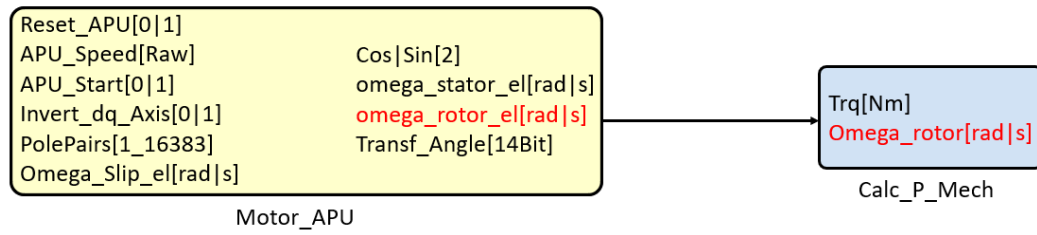


Figure 4.10: Zoom on the blocks to calculate of Mechanical Power dSPACE (dq) model.

Starting from the left block it is possible to notice that in this block are calculated respectively the rotor electrical speed $\omega_{rotor\ el}$ and the stator electrical speed $\omega_{stator\ el}$. In Figure 4.10 are represented the enlarged blocks that dSPACE uses to calculate the mechanical power.

The rotor speed ω_r is equal to:

$$\omega_r = \frac{\omega_{r(e)}}{pp} \quad (4.3)$$

where $\omega_{r(e)}$ is the rotor electrical speed and pp is the number of Pole Pairs.

The (4.3) is used to evaluate the mechanical power, indeed it is equal to:

$$P_{mech} = T_{em} \cdot \omega_r \quad (4.4)$$

where T_{em} is shown in the 2.45.

$$P_{mech} = T_{em} \cdot \omega_r \quad (4.5)$$

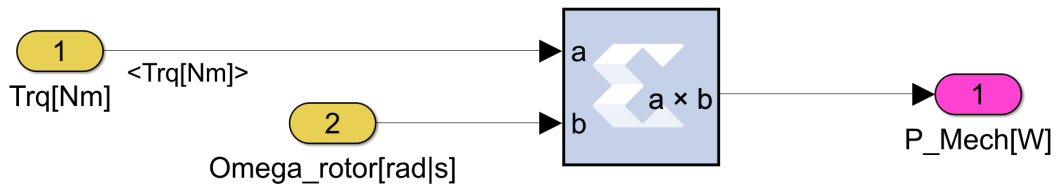


Figure 4.11: Mechanical Power dSPACE (dq) model block.

As it is possible to see from the Figure 4.9 and 4.11, the dSPACE model does not have the coefficient that transforms the rotor electrical speed into rotor mechanical speed and for this reason, the mechanical power is not evaluated correctly.

This inconsistency was pointed out to the dSPACE support they will fix this bug.

The other inconsistency concerns the calculation of the stator voltage in the q axis. Indeed debugging the model it is possible to see that the following term does not appear in the calculation blocks:

$$\frac{1 - \sigma}{\sigma \cdot T_r} \cdot i_{sq} \quad (4.6)$$

To verify this theory, the dSPACE (dq) model was represented in Simulink. From this check, it immediately became clear that there was an inconsistency in the dSPACE model. Also in this case, the dSPACE support will provide the model without this bug.

Pending their answer, the dSPACE (dq) model has been modified with the term represented in 4.6 and the comparison between the off-line Simulink model and the real-time dSPACE model is represented below.

As for the ($\alpha\beta$) model, also in this case the quantities represented are:

- Stator current;
- Rotor speed.

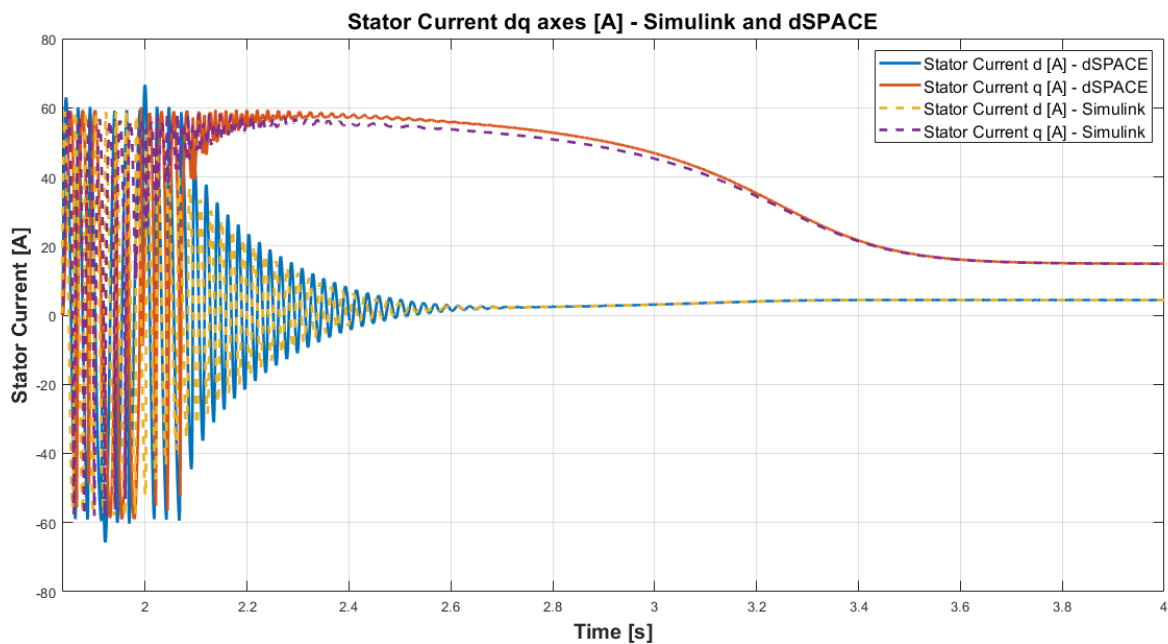


Figure 4.12: Stator current Simulink and dSPACE real-time (dq) model.

To get a clearer idea, it is possible to observe individually the stator currents in axes d and q .

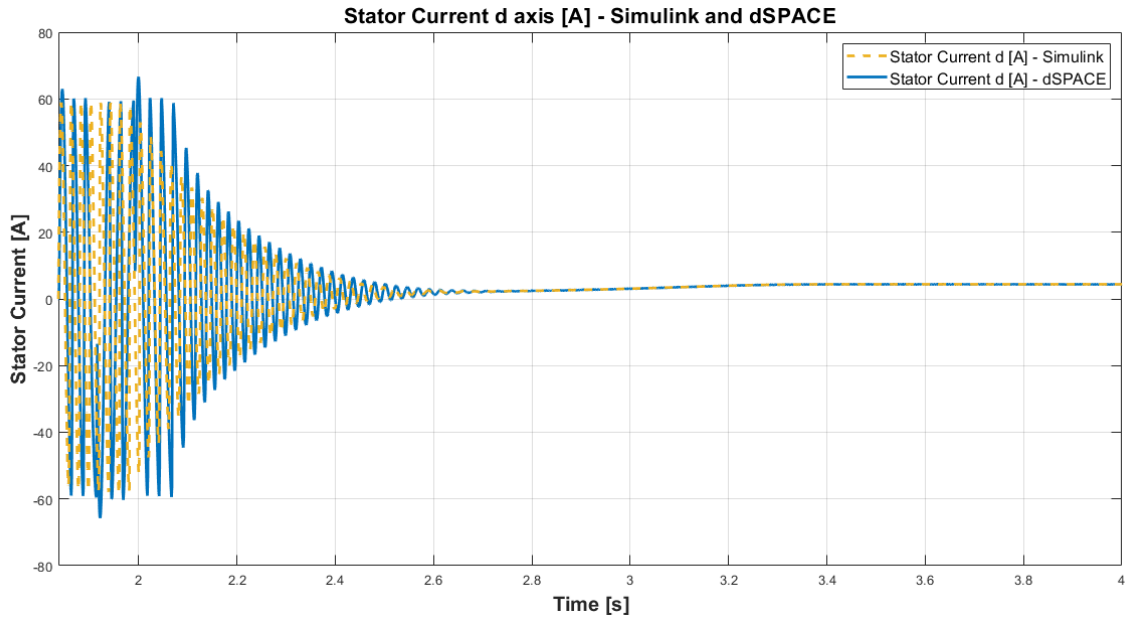


Figure 4.13: Stator current d-axis Simulink and dSPACE real-time (dq) model.

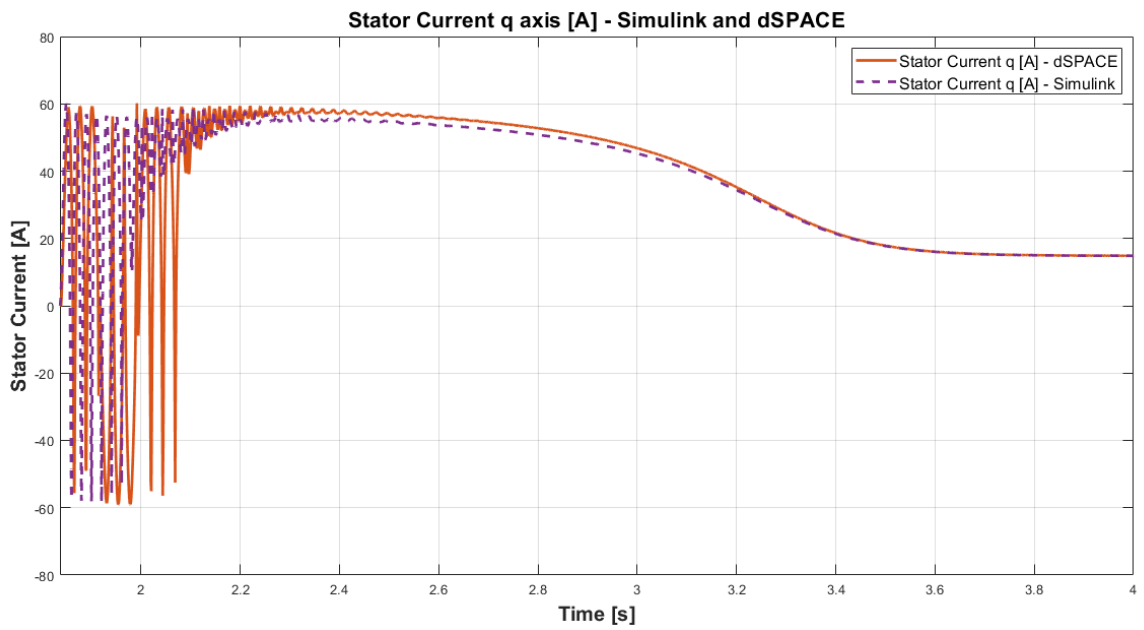


Figure 4.14: Stator current q-axis Simulink and dSPACE real-time (dq) model.

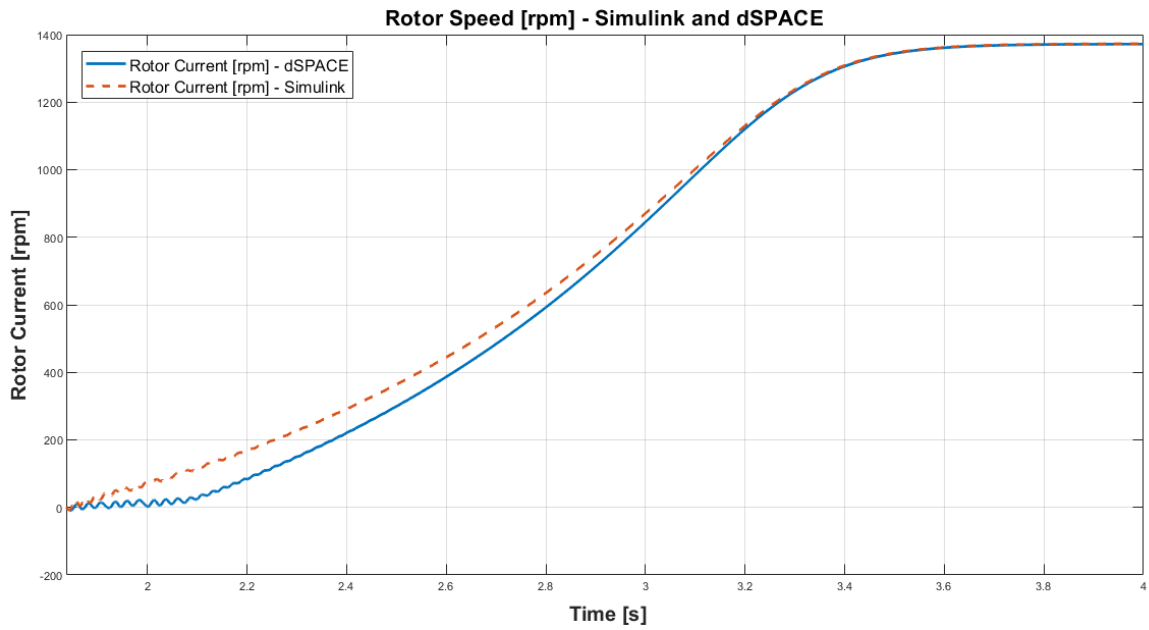


Figure 4.15: Rotor Speed Simulink and dSPACE real-time (dq) model.

While for the $(\alpha\beta)$ model a perfect overlap was found, for the (dq) model this was not possible, probably because this model is little used in HIL. It's necessary to deepen the model further and the dSPACE support will also resolve this inaccuracy.

Chapter 5

Validation of the dynamic model

In this chapter, a real IM has been tested on a dedicated test bench in Politecnico di Torino's laboratories to get a preliminary validation of the proposed models. The values of the induction motor are evaluated. These values are calculated with no-load and locked rotor tests.

To make these tests, the instrumentation used is the induction motor, the TPS/T, the current transducers and the HBM.

In order to study the dynamics of the system, the tests were carried out with no-load and with different values of voltages and frequencies.

5.1 Model of the system

The instrumentation used is located in the Politecnico di Torino's laboratories. The system used to carry out the experimental tests is illustrated in the following figures.

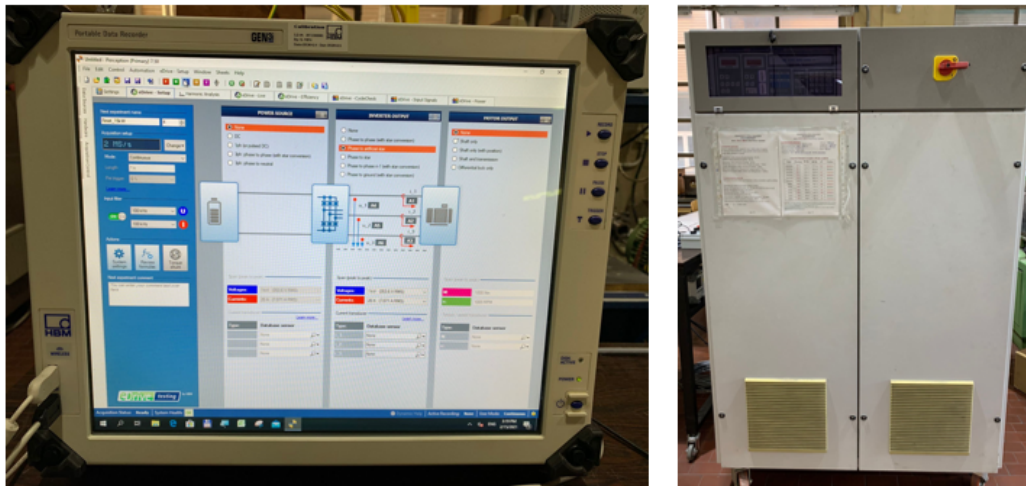


Figure 5.1: HBM and Single-three phase power source 40kVA.

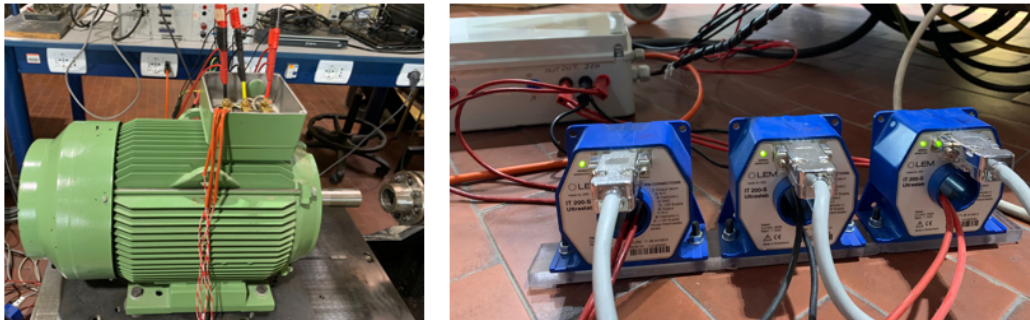


Figure 5.2: Induction motor and Current transducers.

Figure 5.1 shows the HBM and Single-three phase power source 40kVA.

The HBM is a data recorder and is combined with a PC Windows. In the laboratory, the HBM available is the model Gen3i; it has 8GB RAM and a processor Intel i3. The software used to acquire the data is Perceptions. The HBM has two operative modes: continuous or transitory. The measured data are sent directly on the SSD or an external PC. The sampling time can be set and it is tunable [12].

The TPS/T 40kVA is a single-three phase AC and it provides a sinusoidal waveform. The frequency and voltage can be programmable. The interval of a frequency is between 10Hz and 80Hz and that of the voltage is from 0VAC to 300VAC phase-neutral [13].

In Figure 5.2 are shown the induction motor and the current transducers.

The induction motor used for the experimental tests is FIMET HMA160L4 and it is a squirrel cage with a rated power of 15kW and with 4 poles. It can be powered Y/ Δ . The tests for the

comparisons are made with no-load and with different power supply.

The current transducers used to made the tests are three. The operating temperature is from -40°C to 85°C . It is used for very high precision current measurements. The secondary connector is characterized by 9 pin-D-sub [14].

The complete system can be represented with the following scheme:

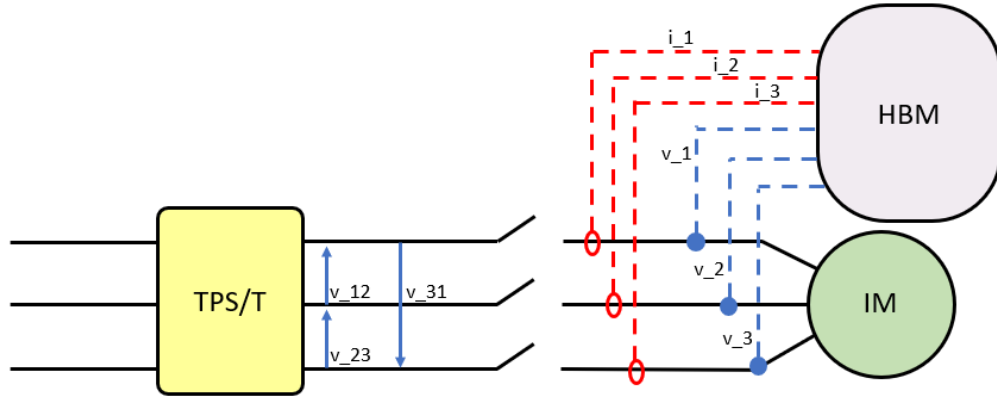


Figure 5.3: Schematic representation of the test bench.

The three sinusoidal voltages v_{12} , v_{23} and v_{31} exit from the TPS/T. On the legs of the model are represented the three current transducers that measure the line currents i_1 , i_2 and i_3 and these currents are read by the HBM. The voltages v_1 , v_2 and v_3 are also read by HBM.

5.2 Calculation of machine parameters

To evaluate the machine parameters, it is necessary to start from the no-load and locked-rotor tests. Thanks to these, in fact, it is possible to calculate the inductances and the resistances of the motor. The theory of the tests is entirely described in subsections 2.7.1 e 2.7.2.

From the no-load test, the mutual inductance and the iron resistance is calculated. In this thesis, the iron losses and the magnetic saturation of the machine are not considered, but the iron resistance R_{fe} and the magnetizing reactance X_m are essential for the calculation of other machine parameters. The equations used to calculate these quantities are shown in the 2.58.

The other parameters of the motor are calculated with the locked-rotor test. As described in subsection 2.7.2, the stator and rotor inductances, X_s and X_r , and the stator and rotor resistances, R_s and R_r , are calculated from the no-load test. The equations used are the 2.59 and 2.60.

In the figures below some instruments used during the various tests are clearly depicted.

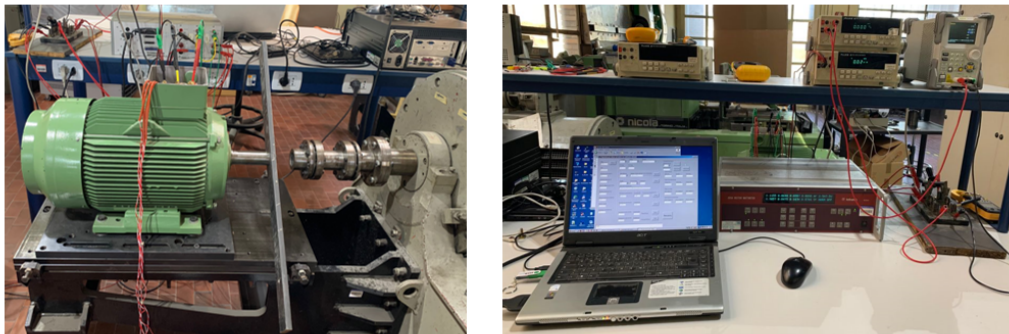


Figure 5.4: Instrumentations used during the no-load and locked rotor tests.

The data of the IM provided by the datasheet are reported in Table 5.1:

Table 5.1: Data of the IM.

<i>Motor type</i>	<i>HMA160L4</i>	<i>Company</i>	<i>FIMET</i>
<i>Power [kW]</i>	<i>15</i>	<i>Connection</i>	<i>D</i>
<i>Voltage [V]</i>	<i>400</i>	<i>Current [A]</i>	<i>30</i>
<i>Speed [rpm]</i>	<i>1470</i>	<i>Frequency [Hz]</i>	<i>50</i>
<i>Poles number</i>	<i>4</i>	<i>Test supply</i>	<i>SIN</i>

The no-load and locked-rotor tests are performed in Politecnico di Torino's laboratories. The results of the tests are reported in Table 5.2 and in Table 5.3.

Table 5.2: No-load test results.

<i>V</i> _{line} [V]	<i>E</i> _{line} [V]	<i>I</i> _{line} [A]	cos(ϕ)	<i>P</i> _{tot} [W]	<i>P</i> _{cu} [W]	<i>P</i> _{iron+mec} [W]
417.6	417.4	16.0	.053	615.3	144.7	470.6
400.2	399.9	14.1	.053	517.0	112.3	404.7
374.1	373.9	11.7	.053	403.6	77.0	326.5
348.1	347.9	9.9	.054	326.7	56.4	270.3
304.5	304.4	8.2	.058	252.3	37.9	214.4
261.0	260.9	6.7	.064	197.1	25.9	171.1
217.6	217.5	5.5	.076	157.1	17.1	139.9
174.1	173.9	4.3	.095	123.9	10.7	113.3
125.9	125.8	3.1	.152	102.2	5.4	96.7
87.1	86.9	2.2	.247	84.1	2.9	81.3
43.8	48.6	1.6	.551	67.5	1.5	66.0

Table 5.3: Locked-rotor test results.

<i>I</i> _{line} [V]	<i>V</i> _{line} [V]	<i>P</i> [W] [A]	cos(ϕ)	<i>V</i> at T° [V]	<i>P</i> at T° [W]	cos(ϕ) at T°
12.1	34.2	272.7	.382	35.1	319.9	.436
20.9	50.9	797.2	.433	52.6	930.1	.489
27.9	64.2	1418.9	.458	66.5	1643.9	.512
38.6	84.3	2716.3	.482	87.4	3128.4	.535

The stator resistance is equal for the two tests. Applying the 2.58, 2.59 and 2.60 the main parameters of the IM are calculated and they are shown in the table 5.4:

Table 5.4: Parameters of the Induction Motor FIMET HMA160L4.

Parameters of the Induction Motor FIMET HMA160L4	Value
<i>Stator Resistance</i> (Ω)	0.191
<i>Rotor Resistance</i> (Ω)	0.418
<i>Stator Inductance</i> (mH)	53.589
<i>Rotor Inductance</i> (mH)	54.446
<i>Mutual Inductance</i> (mH)	52.160
<i>Pole Pairs</i>	2
<i>Total Inertia</i> (kgm^2)	0.19

5.3 Validation of experimental data

After the first phase of the setting up of the test bench, the experimental tests are carried out. The test bench used is represented in the sketch of the Figure 5.3. The measurements of all signals necessary to the implementation of the model of the motor were made with a no-load test and with a delta connection.

In this phase of the work, two simulations were considered:

- $30V_{ph}$ - $50Hz$ with ramp acceleration and abrupt stop;
- $30V_{ph}$ - $50Hz$ with step acceleration and abrupt stop.

Considering the perfect overlap with the dSPACE model in the simulations of Chapters 3 and 4, the validations of the experimental data were made considering only the Simulink model.

On HBM it is possible to see voltages and currents over time. The following values are read at the same RMS value of concatenated voltages as measured with HBM.

Table 5.5: Validation of experimental data.

$V_{lineRMS}$ HMB (V)	$I_{lineRMS}$ Simulink (A)	$I_{lineRMS}$ no-load (A)	$I_{lineRMS}$ HBM (A)
51.6	1.8	1.7	1.9

The results reported in the table refer to the simulation made with Simulink with the same fed and to the interpolation line of the current values reported in Table 5.2.

In the first case, the stator current of the simulations 30V - 50Hz with ramp acceleration is shown. To get a clearer picture, only one phase of the current is shown.

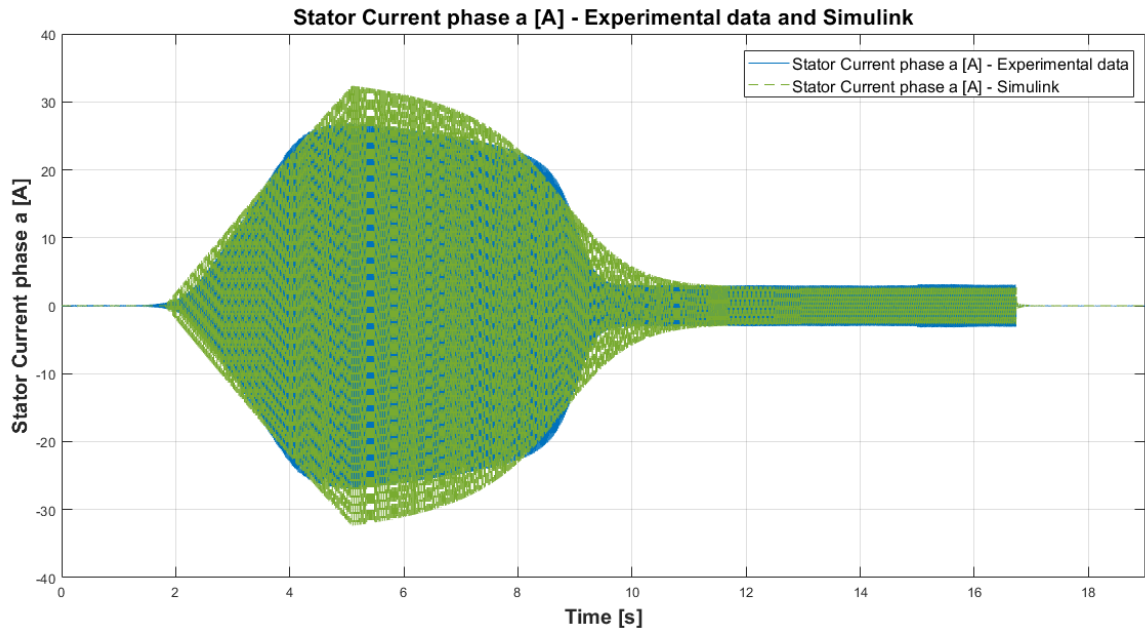


Figure 5.5: Stator Current 30V - 50Hz with ramp acceleration.

Zooming on the starting transient and on the steady state, it results clear that the two results are overlapping.

- Starting transient:

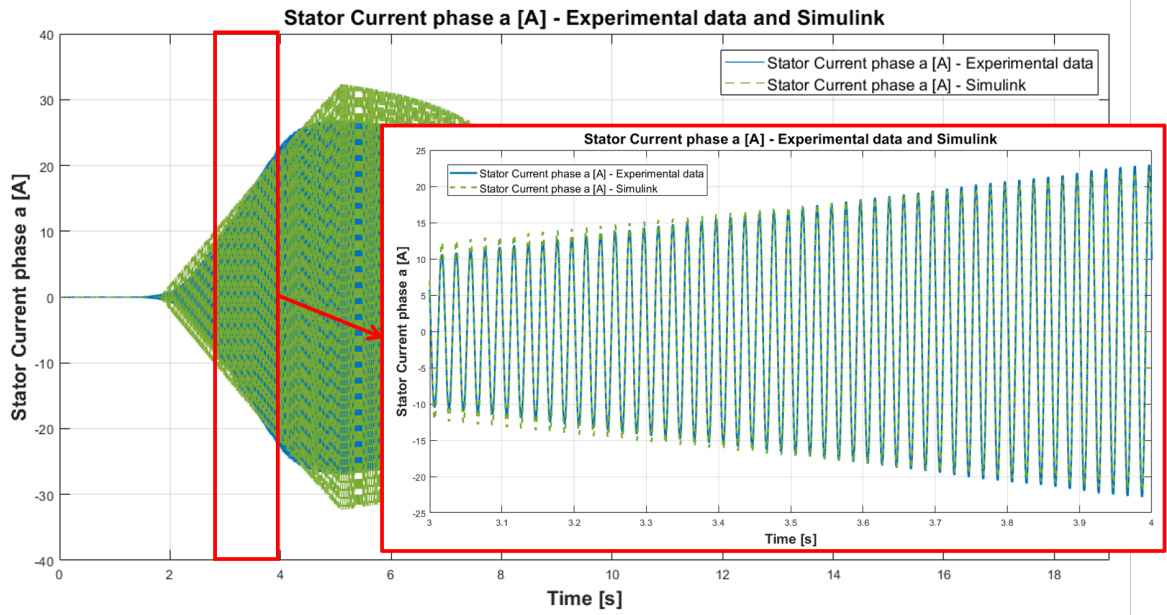


Figure 5.6: Zoom starting transient - Stator current 30V - 50Hz with ramp acceleration.

- Steady state:

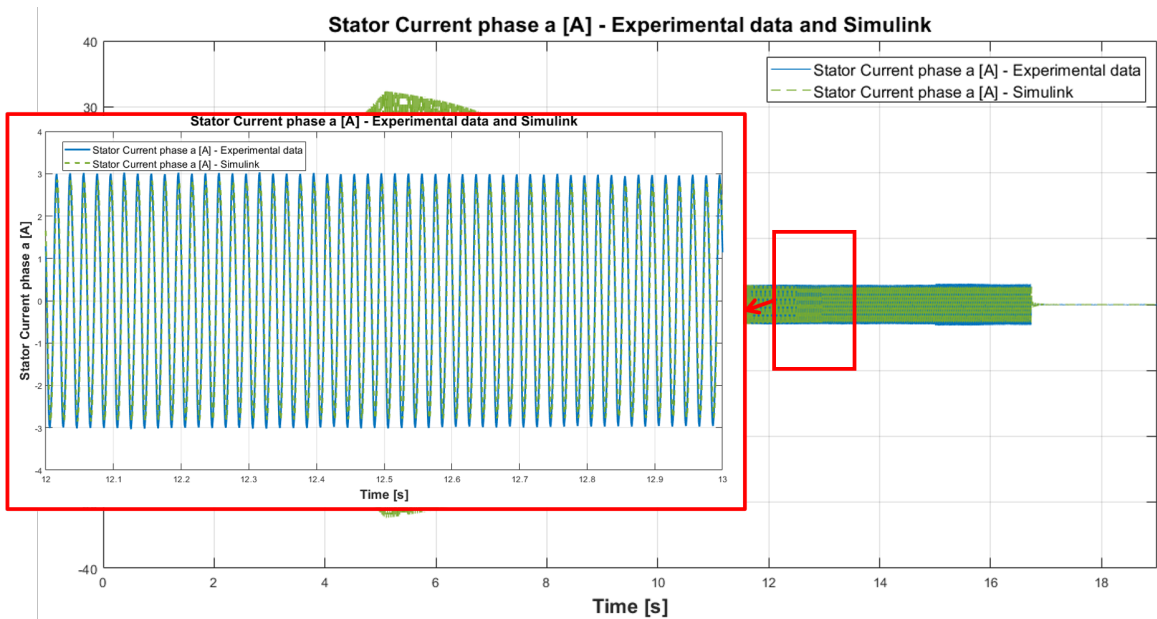


Figure 5.7: Zoom steady state - Stator current 30V - 50Hz with ramp acceleration.

In the second case, the stator current of the simulations 30V - 50Hz with step acceleration is represented.

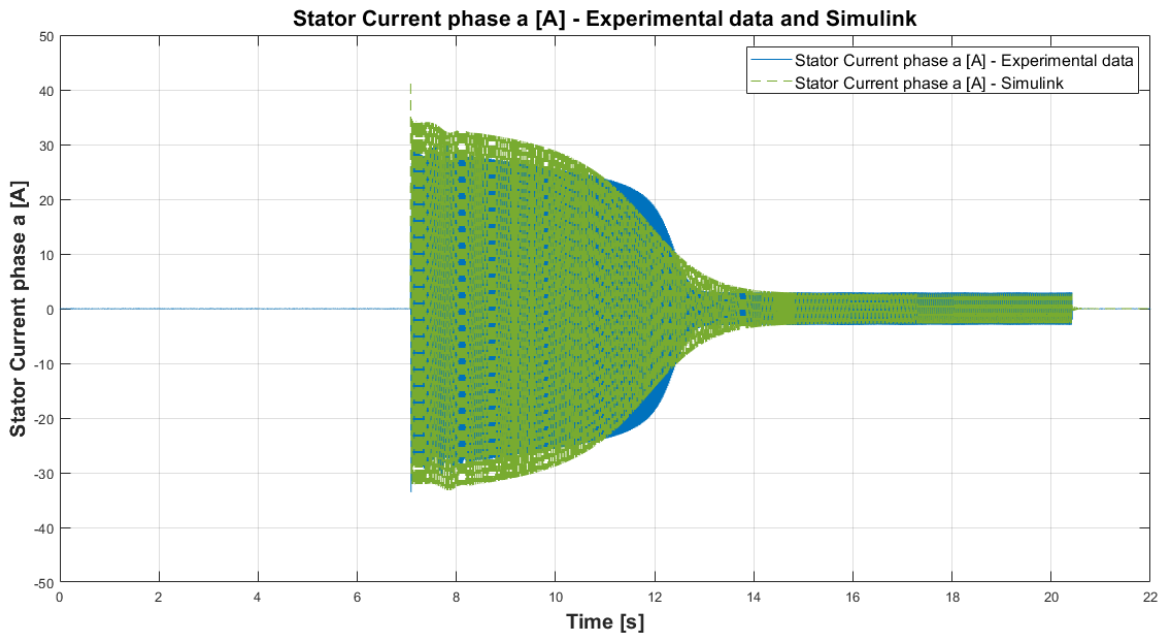


Figure 5.8: Stator Current 30V - 50Hz with step acceleration

Also in this case, zooming on the starting transient and on the steady state, it results clear that the two results are overlapping.

- Starting transient:

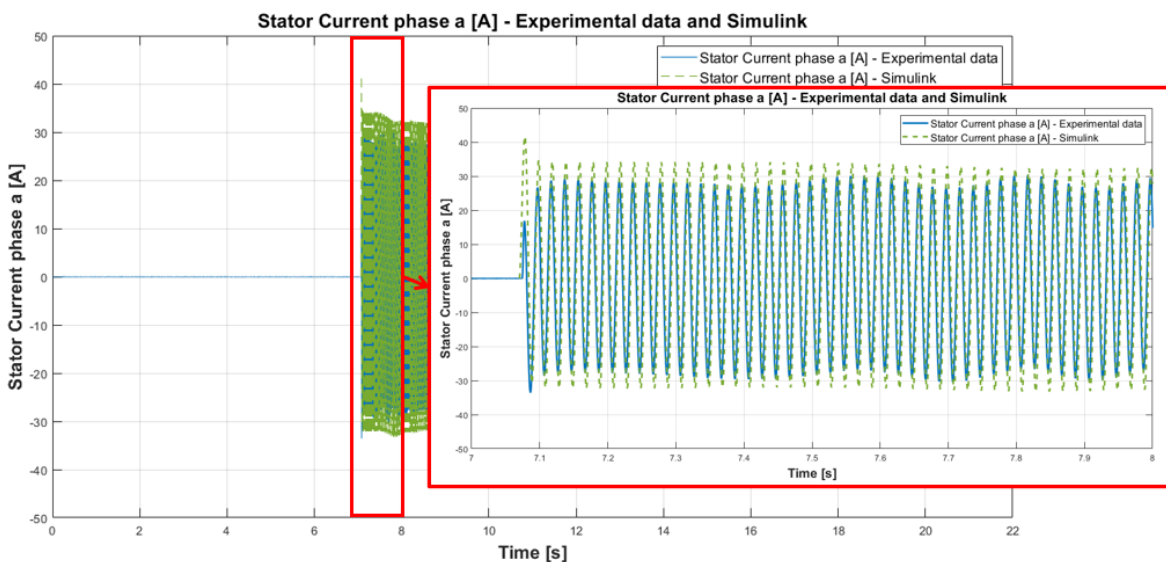


Figure 5.9: Zoom starting transient - Stator current 30V - 50Hz with step acceleration.

- Steady state:

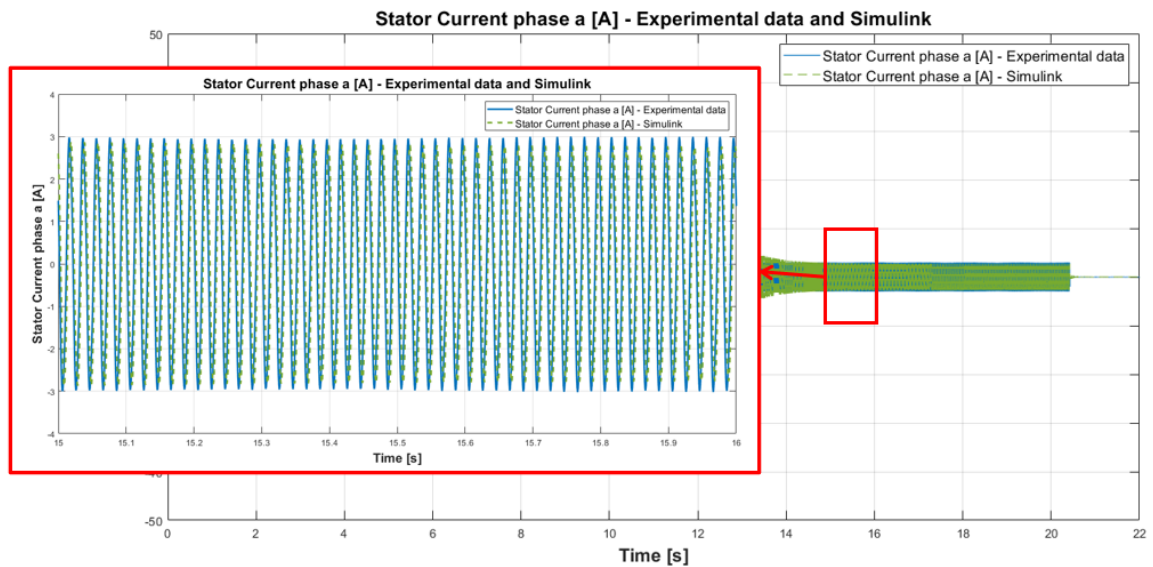


Figure 5.10: Zoom steady state - Stator current 30V - 50Hz with step acceleration.

From the Figure 5.6, 5.7, 5.9, 5.10, it is possible to see the different accelerations and the abrupt stop. The waves don't perfectly overlap and the Simulink model has slightly higher values in the starting transient because in this model iron losses and magnetic saturation are not considered. In addition to these, mechanical losses and friction are also not considered. In the motor of the test bench, the stator current is higher than in the simulation with the Simulink model due to the presence of friction.

Chapter 6

Conclusions and next steps

In this thesis work, the mathematical model of the Induction Motor (IM) is analysed and the equations of the machine have been described. After this, the IM model was developed in Matlab/Simulink and dSPACE environments. dSPACE is a software that is used for Hardware in the Loop (HIL) simulations. Through the use of ControlDesk and ConfigurationDesk it was possible to evaluate the behavior of the IM in real-time.

The first goal of this work was to model the IM in the $(\alpha\beta)$ reference frame in Matlab/Simulink and later in dSPACE. Once this was done, the dSPACE model was analysed and the model was debugged. After a careful analysis, it is possible to say that Matlab/Simulink and dSPACE respond in the same way.

Then, the model was developed in the (dq) reference frame and, as for the model in the $(\alpha\beta)$ reference frame, also in this case it was first modelled in Matlab/Simulink and then in dSPACE. The debug of the dSPACE (dq) model of the IM was more complex since in the model there were some incongruences, recognized by the dSPACE support. For these, the Matlab/Simulink and the dSPACE models are not perfectly overlapped and this is due to the many delays and bits dSPACE uses.

In Matlab/Simulink also the mathematical model of the Voltage Source Inverter (VSI) has been developed. The VSI was used to feed the motor and see its behaviour.

In this work, the motor was developed without modelling the iron losses and the magnetic saturation and no account was taken of the friction.

In the future, to have a more complete machine modelling, it would be appropriate to make an IM model with these characteristics.

One could think of feeding the IM with a Voltage Source Inverter (VSI) and not with three sinusoidal voltages.

VSI can be useful for future activities related to engine control and can be implemented with Pulse Width Modulation (PWM).

Bibliography

- [1] Hussein Khreis, Deflorio Andrea, and Miguel Ruiz De Larramendi. *Sensitivity Analysis for Induction Machine Manufacturing Tolerances in EV and HEV*. IEEE, 2015.
- [2] Kavita B. Hunasikatti, Raghuram L Naik, and Basayya V Hiremath. *Implementation of FPGA Based Closed Loop V/f Speed Control of Induction Motor Employed for Industrial Applications*. IEEE, 2018.
- [3] Rik De Doncker. *Electric drives analysis, modeling, Control (power Systems)*. Springer, 2011.
- [4] Andrea Cavagnino. *Macchine Elettriche II*. 2018.
- [5] Antonino Fratta. *Dispense del corso di Conversione Statica dell'Energia Elettrica*. 1998.
- [6] Sandro Rubino. *Controllo di tensione Inverter Trifase VSI*. 2020.
- [7] dSPACE GmbH. *XSG Electric Library*. dSPACE GmbH, Version 19.2 - 01 2020.
- [8] https://www.dspace.com/en/inc/home/products/hw/simulator_hardware/scalexio/ds6602-fpga-base-board.cfm#175_55653.
- [9] dSPACE GmbH. *FPGA Basic Training*. dSPACE GmbH, 2020.
- [10] Xavier Guillaud, M. Omar Faruque, and Alexandre Tenenge. *Applications of Real-Time Simulation Technologies in Power and Energy Systems*. IEEE, 2015.
- [11] Nguyen Phung Quang and Jörg-Andreas Dittrich. *Vector Control of Three-Phase AC Machines*. System Development in the Practice. Springer, 2015. ISBN: 9783662469149.
- [12] <https://www.hbm.com/it/4483/genesis-highspeed-mainframes-with-integrated-pc/>.

- [13] *<http://www.elettrotestspa.it/wp/wp-content/uploads/2015/03/Brochure-TPS40K.pdf>.*
- [14] *<http://www.farnell.com/datasheets/2150002.pdf>.*